Bar-Ilan -

Yeshiva University

Summer Science Research

Internship Program 2019

INTRODUCTION

The Bar-Ilan University-Yeshiva University Summer Science Research Internship Program is an amazing research opportunity for undergraduate men and women, allowing them to contribute to the forefront of science research taking place in Israel. Generously supported by former chairman of Bar- Ilan's Global Board of Trustees, Dr. Mordecai D. Katz, and his wife Dr. Monique Katz, and by the J. Samuel Harwit, zt"l & Manya Harwit Aviv Charitable Trust, students gain invaluable laboratory skills, along with an unforgettable summer experience.

Program Director: Professor Arlene Gordon
Av and Em Bayit: Rav Chaim and Ronit Goldberg

Table of Contents

Editor-in-Chief: Aleeza Katz

Brain Sciences

(L-R) Arina Soklakova, Sara Ekaireb, Rachel Retter, Aleeza Katz, Ashley Galitzer, Esther Stern, Albert Dweck

Further Insight in 'Aha'; A Look into Forward and Backward Remote Associates

Esther Stern
Advised under Dr. David Anaki

There is much in the way of insight that remains unknown, resulting in a multitude of current research on the subject matter. Insight can be described as "a sudden change in or the formation of a concept or other type of knowledge representation, often leading to the solution of a problem" (Kounios & Beeman 2014). A further understanding of insight can be achieved by discussing what it is not an analytic solution. Insight solution is distinguished from an analytic solution in that the former is accompanied by a burst of emotion that includes a positive surprise (Kounios & Beeman 2014). This burst of emotion, the eureka moment, is referred to as the 'aha' moment. This is a defining feature of insight, which is largely borne via unconscious processing. Therefore, when insight occurs it seems disjunct from the conscious stream of thought which is disrupted by the 'aha.'

In later neuroscience studies, the creation of problems that are solvable by insight (Bowden & Jung-Beeman 2003a) has been a productive way to quantify insight as well as creativity. Bowden and Beeman used a set of remote associate problems made up of three words each (e.g cottage, swiss, and cake). The participant is then tasked with finding an associate word that forms a compound or familiar phrase with the given three words (e.g cheese). Bowden and Jung-Beeman's paradigm is modeled after Mednick's remote associates test of creativity (Mednick 1962). Although predominantly used to quantify creativity,

Mednick's Remote Associates Test (RAT) is one of the more direct ways of studying insight.

There are two types of remote associate word sets: forward (e.g given 'cheese' and looking for 'cake' in response) and backward (e.g given 'cheese' and looking for 'swiss' in response) remote associates. It is generally thought that forward associations are stronger because they are more direct, whereas backward associates need to be flipped to generate an answer. This brought us to theorize that this could also be the case with remote associates that measure insight. This prompted a further look into results from insight remote associate tasks provided by Bowden and Beeman. Our analysis strongly suggested a difference between the strength of forward and backward association. Thus, a study was warranted to further investigate this difference between forward and backward association in insight, this time with an emphasis on seeing its effect on 'aha' moment and accuracy.

In the present study, 40 remote association triplets were presented to each participant via computer. Half of the triplets were forward associates and the other half were backward associates. Each triplet was associated with a target word, and was chosen based on strength from Nelson and Bowden Beeman (Nelson 1998). Participants were given 20 seconds to think of the target word. If they had succeeded in generating the target word within the allotted time, we referred to this as 'insight'. Participants were then asked two questions: Whether they experienced an 'aha' moment, and how confident they were in their answer choice.

We did not run statistical analysis on the results; rather, we looked for informative trends in the data. Results show that both 'aha' moment strength and accuracy rates are greater in forward association triplets as compared to backward association triplets. This supports our theory that there exists a forward association advantage in the context of insight, as shown through both increased aha moment strength and accuracy. Further research should be done to find the neural correlates of insight as it relates to forward and backward remote associates.

Figure 1: Accuracy in both forward and backward associations in correct and incorrect responses with insight.

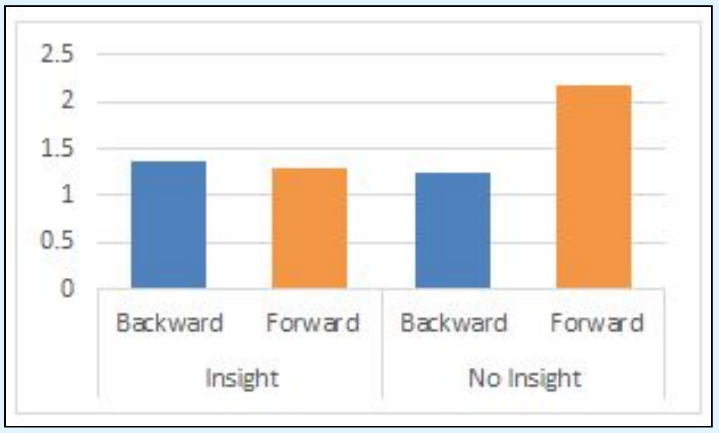

Figure 2: 'Aha' moment in the correct responses with insight and in the incorrect responses without insight with forward and backward associates.

Bowden, E. M., & Jung- Beeman, M. (2003a). Normative data for 144 compound remote associate problems. *Behavior Research Methods, Instruments, & Computers,* 35 (4), 634-639.

Kounios, J., & Beeman, M. (2014). The Cognitive Neuroscience of Insight. *Annual Review of Psychology,* 65, 71–93. doi: 10.1146/annurev-psych-010213-115154

Mednick, S. A. (1962). The associative basis of the creative process. *Psychological Review*, 69, 220-232.

Nelson, D. L., McEvoy, C. L., & Schreiber, T. A. (1998). The University of South Florida word association, rhyme, and word fragment norms. http://www.usf.edu/FreeAssociation/

Effect of Parietal Activation on Episodic Memory: A New Paradigm

Rachel Retter

Advised under Dr. David Anaki

Recently, the neuropsychological community encountered an intriguing puzzle. For years, it was considered established that the parietal cortex was not involved with episodic memory. This was supported by numerous cases of patients with parietal lesions who did not have significant episodic memory deficits. However, modern brain imaging technologies yielded findings showing that the parietal cortex is in fact frequently activated during episodic memory retrieval.

How to approach this apparent contradiction? Recent developments have helped clarify the true role of the parietal cortex in connection to episodic memory. The advent of event-related fMRIs and new neuropsychological studies have enabled scientists to distinguish between particular types of memory processes and identify how each are related to parietal cortex activations. For example, while patients with parietal lesions did not experience actual amnesia, they did exhibit a decrease in certain memory functions such as vividness and abundance of detail, remembering states and memory confidence, as compared to a control group.

With this newfound information, researchers hypothesized several models for how parietal activation affects episodic memory. While each model is supported by recent neuropsychological test results, most acknowledge limitations and inconsistencies. Additionally, the amount of studies done on this topic is scant, and "future research might bring different evidence to bear on it."[1]. For these reasons, this area of research is a worthwhile realm to explore, and will likely yield new and exciting results.

In the present study, we aim to create a paradigm which can be used to test these different models and further explore this field. This paradigm proposes the use of arithmetic tasks that activate the angular gyrus (AG), a region of the parietal cortex, to potentially enhance episodic memory. It has long been established that basic arithmetic tasks activate the AG, which is associated with the rote verbal memory used to recall familiar multiplication tables and addition problems. For this study, all equations had a sum that was less than ten in order to maximize rote memory, as opposed to more challenging problems, which would be less familiar and could activate problem solving and working memory.

The benefits of this paradigm are twofold. Firstly, cognitive tasks are much less costly and time consuming than most brain scans. Secondly, most brain scans cannot activate a region in the brain; they merely allow us to observe brain activation, typically during a particular

[1] Cabeza, Roberto & Ciaramelli, Elisa. The parietal cortex and episodic memory: an attentional account. *Nature Reviews Neuroscience* 9, 613 (2008)

cognitive task. In contrast, the arithmetic task activates the AG, potentially enhancing its function.

The present study is composed of three parts. The first is an encoding task, where the subject is presented with 48 words to memorize. The second part is an arithmetic task, where the subject is presented with basic arithmetic equations and is asked to determine whether the answer presented is correct or incorrect. This is meant to activate the AG, and potentially enhance episodic memory function for the third task, which is a retrieval task. There were also two control tasks which did not activate the AG (letter substitution task and blank task.) In the third part, the subject is presented with 48 words, some of which are from the previous list and some of which are new. Upon seeing each word, the subject determines whether they recall the word (have a particular image or sensory association with it in addition to remembering that it was in the previous list), know the word (do not have a particular association with it but remember that it was in the previous list) or do not remember it at all.

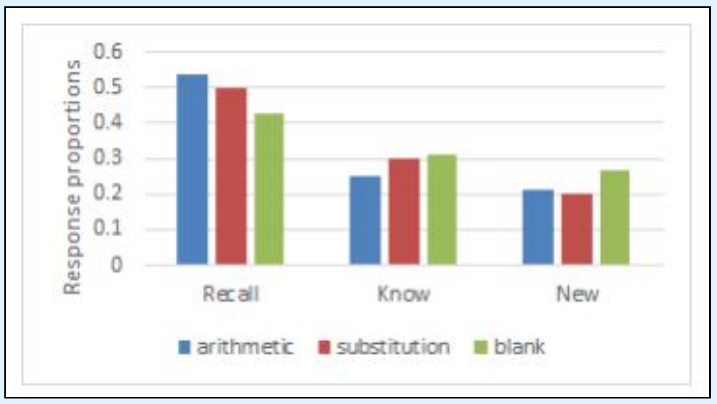

Figure 1: Memory Retrieval as a function of tasks.

Because the groups were small (7-8 subjects), we did not run statistical analysis on the results; rather, we looked for trends to point us in the right direction for future studies. “Recall’’ rates (vivid details and associations) were higher in the arithmetic task (.54) than in both control groups (.50 and .43), while the opposite was true for “know” rates (familiarity without associations). These results support the theory that arithmetic tasks activate the AG and enhance the memory functions specifically associated with that area (i.e., richness and abundance of detail and context). Future studies may test this paradigm further as a user friendly and effective mechanism to explore the relationship between the parietal region and episodic memory.

Evaluating the Relationship between Fluency Measured at Different Levels of Reading and Reading Comprehension in English as a Foreign Language Among Arabic Speaking Learners

Aleeza Katz
Advised under PhD candidate Mona Saba, Professor Sharon Armon-Lotem, and Dr. Carmit Altman

Fluency while performing a reading task is the combination of speed and accuracy. Thus far, research has focused on the relationship between accurate word recognition and improved reading comprehension, while marginalizing the importance of speed. Therefore, fluency was not a primary concern in the design of reading development research for First language (L1) or Foreign language (FL). Moreover, in cases where fluency was tested, previous research defined fluency as the outcome of reading rate and accuracy at the word level (word reading fluency, hereafter WRF), while ignoring Text/Oral reading fluency (TRF).

This previous research has had a negative impact on reading theory. Children who exhibit typical isolated-word decoding accuracy skills, but lack the ability to perform elementary text-based comprehension tasks often do not receive appropriate attention.

Additionally, fluency at both the word and text levels is an essential component of reading comprehension (RC) in both L1 and L2, yet, much remains unknown about whether word fluency and text fluency reflect one fluency construct or two independent constructs.

Mona Saba's PhD research addresses the lack of current research on this topic and investigates fluency among a sample of Arabic speaking learners of English as a foreign language (EFL) in grades 6, 7, and 8 at three different levels: metalinguistic awareness fluency, WRF, and TRF. This study explores the relationship between these three skills and RC in EFL through parallel Arabic and English speed and accuracy measures. Additionally, the present study addresses metalinguistic fluency in Arabic L1 and its relationship to the same skills in EFL, as well as to WRF and TRF in EFL. Finally, this research investigates whether fluency measured at the different levels enhances or changes our understanding of reading development in EFL than parallel speed and accuracy measures.

This study is expected to provide a deeper understanding of the nature of fluency in EFL, an area of research that is currently lacking sufficient attention, as well as of the nature of development of fluency in EFL among Arabic speaking learners of EFL.

Integrative Narrative Analysis in Typical Adults and People with Aphasia PWA

Ashley Galitzer
Advised under Dr. Carmit Altman and Professor Sharon Armon-Lotem

This summer, I worked with Dr. Carmit Altman on the integrative analysis of narratives that included narrative structure, grammaticality, and fluency features in typical adults with and without aphasia. The participants were asked to tell a personal narrative about a vacation they went on, and afterwards, their narratives were transcribed and coded into different Analysis of Speech Units (AS Unit; Foster et al., 2000). Each AS Unit was analyzed both for microstructure and macrostructure. We analyzed each AS Unit to see if it had global and local coherence, the amount of clauses and how meaningful they were. We also determined what part of the story scheme was an evaluation, setting storyline or an irrealis (Longacre et al, 1996; Labov & Waletzky, 1997/1982). Then, each clause was rated for grammaticality and each word in the clause was broken down linguistically into: nouns, verbs, adjectives, articles, pronouns, auxiliary verbs, and whether they functioned as fillers, false starts, or discourse markers.

When we were analyzing and coding each narrative, we did not know which participants had aphasia. This was done in order to keep the coder unbiased when analyzing the different texts. After the coding is done, Dr. Carmit Altman who is spearheading this project, will analyze the data and finally reveal to us which adults actually had aphasia. Based on this data, we will be able to identify which features

best characterize the narratives of people with aphasia in comparison to an equivalent control group.

Foster, P., Tonkyn, A. and Wigglesworth, G. 2000. Measuring spoken language: A unit for all reasons. *Applied Linguistics*, 21: 354–375. [Crossref], [Web of Science ®], [Google Scholar]

Longacre, R. E. 1989. Two hypotheses regarding text generation and text analysis. 2. *Discourse Processes*, 12: 413–460. [Taylor & Francis Online], [Web of Science ®], [Google Scholar]

Odor Localization: Strategies and the Neural Mechanisms Underlying Them

Albert Dweck
Advised under Dr. Rafi Haddad

Rodents, specifically mice, have the ability to navigate with the use of the sense of smell. Thus, mice's sense of smell is as important to them as vision is to humans. Odor input is sent through the olfactory system to the portion of the brain that is involved in odor perception. Constructing a map of the mouse brain, with a focus on the olfactory system, will give insight into how mice generate behavior and perception.

After inhaling odorized air into the nasal cavity, odorant molecules interact with olfactory receptors (OR) and trigger neural signals. One OR is expressed per olfactory sensory neuron (OSN), millions of which form a dense sheet called the olfactory epithelium (OE). Each OSN projects one unbranched axon unilaterally to a structure called the glomerulus, which is located in the olfactory bulb. OSNs expressing different ORs project to different glomeruli and thus, the glomeruli are considered the functional units for integrating olfactory information.

Almost all sensory information is topographically organized according to a physical property. This simplifies the sharing of information between the two hemispheres of the brain when the sensory input is not projected bilaterally. Unlike other sensory information, odor information is projected unilaterally and is not topographically organized. Thus, olfactory perceptual unity is puzzling and complex.

The connection that links the two olfactory cortices is facilitated by the anterior commissure (AC). The AC is a fiber bundle of interhemispheric connections which includes those between anterior olfactory cortices (or nucleus; AON) and piriform cortex (PCx). It mediates the bilateral connection between the two hemispheres and allows for the sending of odor information from one lobe to the other. This interhemispheric connection allows mice to compare odor stimuli from each nostril which is the underlying reason why mice are able to orient based on the sense of smell.

A behavioral experiment was designed to understand how mice locate an odor using their sense of smell. A dark empty box was set up, on the floor of which was a 5x10 grid of drawn boxes numbered 1 to 50. With the use a Matlab program, a set of 25 numbers between 1 and 50 was randomly selected. A single trial consisted of one mouse being tested 25 times and the selected numbers were the same between all trials and were not repeated during the same trial. For each of the numbers given in a trial, a drop of water with the scent of orange was placed in that number's box. Afterward, a water deprived mouse was placed into the box

and the time taken for the mouse to find the drop, as well as its behavior throughout the experiment were recorded.

After undergoing multiple trials, the mice began to understand what was expected of them and their experimental times decreased. To understand how mice locate the odor, multiple procedures were performed on select mice. These procedures included plugging one of their nostrils, lesioning one or both of their AONs, and slicing their ACs. The mice were then tested again and their time and behaviors were recorded and compared to the data collected prior to the procedures.

From the data collected so far, it was concluded that when one nostril was plugged, the mice were able to locate the drop, though they did not find it as easily as those with both nostrils open. With regard to lesioning the AON, it was expected that the mouse would act as it does with one nostril closed. However, after the procedure the behavior of the mouse was the same as before, so it was concluded that the AON has no effect on odor localization. Testing with the sliced AC has not yet been conducted, but it is hypothesized that after this procedure the mice will behave as if one nostril is plugged. This would occur because the odor information would not be able to be sent from one hemisphere to the other and no comparison of odor strength through each nostril would be made.

The experiment will be complete when the exact brain region involved in localizing odors is found. Once this is done, electrodes will be placed in these regions to record the neurons while the animal searches for the odor.

Effects of Charismatic Leadership on Brain Synchrony Between Followers: A MEG Study

Sara Ekaireb
Advised under Dr. Avi Goldstein

A fundamental question to both neuroscience and social psychology is to what extent individuals' brains function similarly during naturalistic conditions. Cooperative sociability and capacity to share mental states are not only unique identifiers of human intelligence but indispensable to human development. In order to investigate which human actions enable widely human synchrony, we examined the extent to which exposure to a charismatic (vs. non-charismatic) leader can increase brain synchrony. Charismatic leaders have been shown to facilitate emotional and behavioral contagion in groups. One hypothesis is that charismatic leaders achieve behavioral contagion by increasing the similarity in followers' brain activity, creating a shared perceptual and somatomotor framework for promoting mutual understanding. To this point, functional neuro-imaging techniques have shown that brains "tick together," indicated by higher inter-subject correlation (ISC), in response to captivating visual stimuli such as movies. We use magnetoencephalography (MEG) to directly measure population-dependent neuronal activity at a millisecond resolution to study the brain basis of mutual understanding and cooperation. MEG recordings of 240 sensors were taken while participants viewed videotapes of a professional actor delivering a charismatic speech and a dull (non-charismatic) speech. ISC was taken as the mean correlation of average

frequencies between conditions. As expected, ISCs were higher in response to charismatic vs non-charismatic speech. ISC has been linked to engagement and attentional modulation in earlier studies, but few have investigated what other social, semantic, or perceptual signals trigger similar responses among individuals. In order to investigate which specific charismatic behaviors correlated with the highest levels of ISC, a time course of average ISC was calculated for both the charismatic and dull conditions (Figure 1). The points with the highest ISC were then cross-referenced with the actions of the charismatic speaker in the video tape at those times.

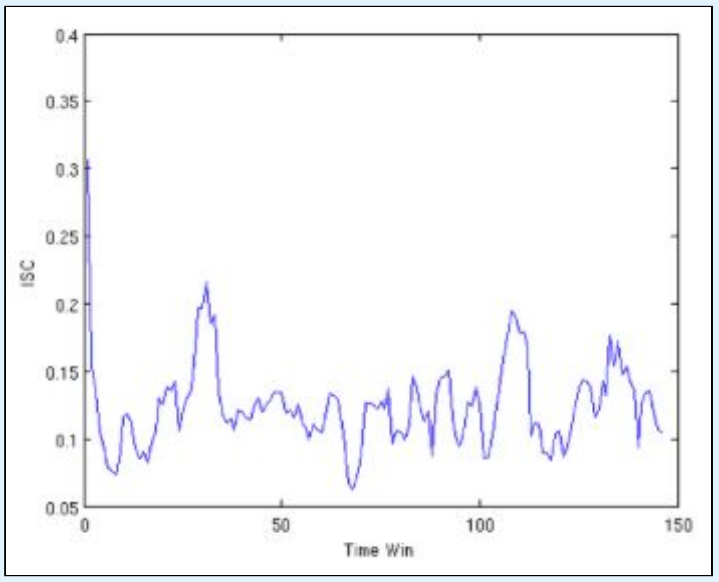

Figure 1: Mean ISC of all 40 subjects as a function of time-course of overlapping time windows of 0.5 seconds every 0.1 second.

Learning Shapes Functional Connectomes From Sensory to Motor Neurons to Generate an Appropriate Behavioral Response

Arina Soklakova
Advised under Prof. Abraham J. Susswein and Dr. Miryam Levy

Learning processes cause modifications at a number of neural sites which lead to numerous adaptive alterations in the behavior. The invertebrate gastropod mollusc Aplysia was used to describe several aspects of long-term memory as its neurons and synapses are readily accessible for examining. Access to most of the neural circuit controlling the behavior allows one to determine the logic and the cellular mechanisms of individual changes that together produce the overall change in behavior.

To examine whether the functional connectome is changed at multiple sites when long- term memory is expressed after learning, we utilized an associative learning task affecting Aplysia feeding, in which it tries, but fails to eat inedible food. Food promotes biting and unsuccessful attempts to swallow, which lead to active rejection and eventually to termination of any responses towards food. Twenty-four hours after training, long-term memory is shown by fewer attempts to bite and swallow food, because the food is actively rejected, and by a decrease in time to stop responding to food that is specific to the taste of food used in the training. After showing the presence of the memory, rejection activity was tested by inducing animals to swallow a cannula, which induces repetitive rejection responses. Rejection was compared in trained and in naïve animals. Trained animals displayed significantly improved rejection (Figure 1), indicating that memory after training with inedible food is partially expressed as a general tendency towards rejection even non-food objects.

Localization of molecular correlates of memory formation to the mechanoafferents and the ability of peptides released by these afferents to bias motor activity to rejection lead us to

test whether rejection activity is increased as a part of memory after animals are trained as described above. To examine whether changes in the synaptic outputs of mechanoafferents contribute to behavioral change after training with inedible food, we first examined in naïve animals the connectivity of a subpopulation of mechanoafferents, the S1 neurons, to 5 followers with different functions (Figure 2) in feeding behavior, expressing long-term memory were compared to those in naïve animals.

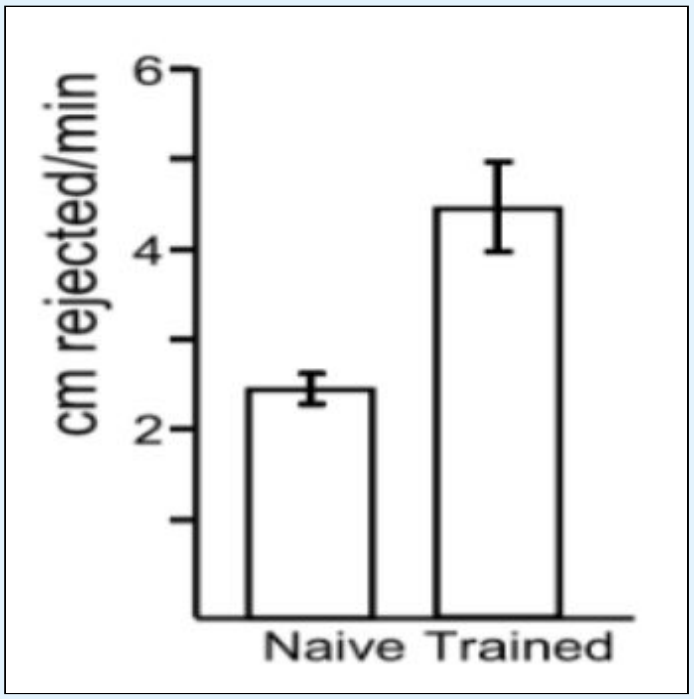

Figure 1: Increased rejection after training and connectivity of S1 and followers. A) Training enhances rejection, as measured by the time required to reject a cannula that was swallowed by the animals. The data show the mean and standard errors of the cm/min rejected in naïve (N = 7) and trained (N = 7) animals (p = 0.002, t = 3.97, df = 12, two-tailed t-test).

In trained animals, there were net increases in excitation to B4/B5 and B61/B62, with a net increase in inhibition to B63. There were no net changes in connectivity to B8a/b and to B31/B32 (Figure 3). These changes are consistent with increased bias to produce rejection.

The different effects of training on connections from S1 neurons to its followers, biasing behavior to rejection, and the finding that cessation of feeding and taste specificity after training is localized to a different ganglion and occurs via a different cellular mechanism, indicates that the functional connectome is regulated by learning at a variety of different sites and by a variety of cellular mechanisms. Access to both presynaptic and postsynaptic neurons in Aplysia allows the subsequent identification of the signals and the mechanisms producing the individual changes that together lead to a global change in behavior.

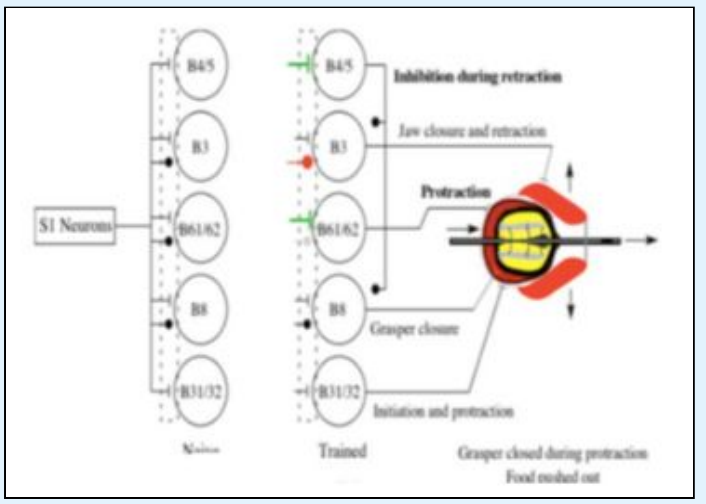

Figure 2: Left: Patterns of synaptic connectivity from S1 mechanoafferents to the 5 followers that were examined. Excitatory synapses are shown by a flat line; inhibitory connections are depicted by circles. Note that 3 followers show exclusively excitatory connections, whereas 3 others show both excitation and inhibition. Right: Changes in connectivity after training. Increased excitation is shown by green shading; increased inhibition is shown by red shading.

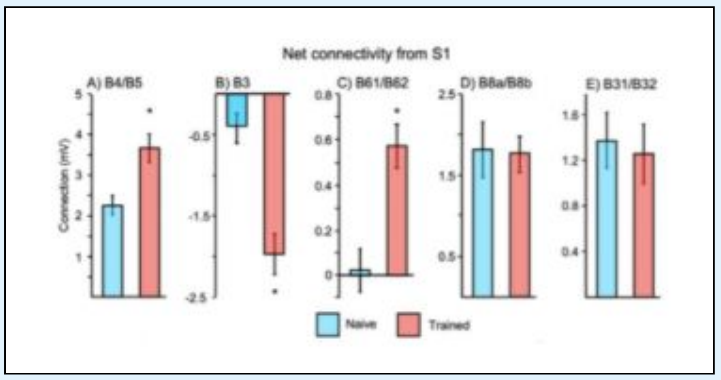

Figure 3: Training biases motor activity toward rejection. Mean net connectivity from S1 mechanoafferents to 5 followers in buccal ganglia from naïve and trained Aplysia. Standard errors are shown. Significant effects are marked with an asterisk.

Life Sciences

(L-R) Mordechai Lis, Elliot Meyers, Jacob Rosenberg, Alexandra Tolmasov, Raquel Klinger, Rachel Mauda

Nonsense Mediated mRNA Decay and Upstream Open Reading Frames in *Arabidopsis thaliana*

Elliot Meyers
Advised under Dr. Orit Shaul and PhD student Miryam Ayala

Cells have many pathways for regulating mRNA. One of these pathways is Nonsense Mediated mRNA Decay (NMD). NMD is a process by which the cell degrades mRNA transcripts with premature termination codons (PTCs), thus allowing the cell to prevent the accumulation of harmful short proteins. NMD can also degrade normal transcripts containing certain cis-elements. In mRNA transcripts, the ribosome attaches to eukaryotic release factor 3 (eRF3) at the termination codon (TC) and the Poly-A-Binding Protein Cytoplasmic 1 (PABPC1) binds to the poly-A tail at the 3' end of the transcript. In non-NMD affected transcripts, the close proximity between eRF3 and PABPC1 allows them to interact (Figure 1A). This interaction avoids NMD and allows proper ribosome recycling after translation termination. In PTC containing transcripts, the TC may be too distant from the poly-A tail to allow eRF3-PABPC1 interaction, thus preventing normal translation termination and ribosome recycling (Figure 1B). Instead, eRF3 interacts with UPF1 (up-frameshift 1), which interacts with UPF

2 and UPF3 (Figure 1C), thereby initiating mRNA degradation.

NMD occurs in transcripts containing PTCs due to nonsense mutations, long 3' untranslated regions (3' UTR), the presence of an upstream open reading frame (uORF), or a few other cis-elements. About 35% of plant genes include a uORF, meaning that they have at least one extra start codon (AUG) before the main AUG. Depending on the Kozak context (a context of base pairs near the AUG which determines the likelihood of translation initiation at that point), the ribosome can start translating at the upstream AUG. When the ribosome reaches the TC of the uORF, it can either release the transcript, or continue to scan the transcript until the main ORF. Ribosomes that are released do not reach the main ORF, thus the presence of a uORF can reduce the translation of the main ORF. If the ribosome is released at the uORF, eRF3 may be a large distance from PABPC1, and this may lead to NMD. The actual distance between eRF3 and PABP1 depends also on mRNA circularization. The 5'-cap of the transcript binds to eukaryotic initiation factor 4E (eIF4E), which binds to eIF4G. The eIF4G factor interacts with PABPC1, thereby causing the mRNA to adopt a circular conformation (Figure 1D).

The question of what determines whether uORF containing transcripts (which can amount to ~35% of all plant transcripts) will undergo NMD or not is not fully understood. The actual distance between eRF3 and PABP in uORF containing transcripts may also be affected by uORF length. Our project was to determine how uORF length affects NMD occurrence. To address this question, we made several constructs that included the strong CaMV35S promoter, the GUS (β-glucuronidase) reporter gene, the NOS (nopaline synthase) terminator, and a 5' untranslated regions (5' UTR) that included uORFs with different lengths (Figure 2).

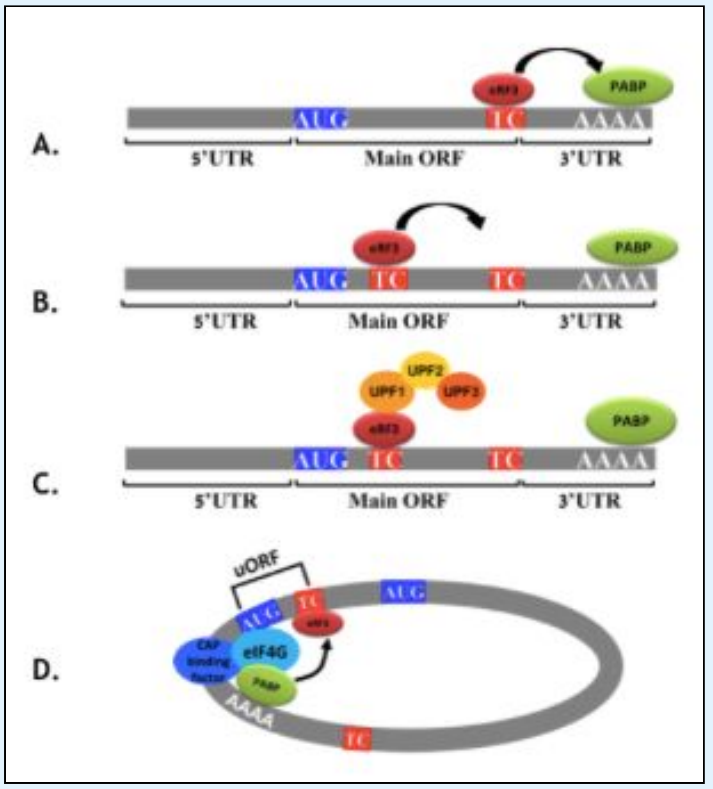

Figure 1: A model of the NMD process.
A. The interaction between eRF3 and PABP allows ribosome recycling.
B. In transcripts with PTCs, eRF3 cannot interact with PABP.
C. Impaired eRF3-PABP interaction leads to eRF3 interaction with UPF1, UPF2, and UPF3, which initiates mRNA degradation.
D. RNA circularization may allow transcripts with short uORFs to avoid NMD due to the proximity of eRF3 and PABP.

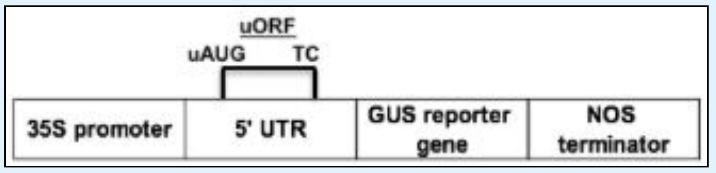

Figure 2. The basic construct in which we introduced uORFs with different lengths.

All the indicated constructs were transformed into the model plant *Arabidopsis thaliana*. For each construct, we collected at least 35 transgenic plants, to account for the "position effect". The seeds of the transformed plants were

germinated on agar plates and harvested at the age of two weeks. The plant material was crushed, and RNA was extracted. This RNA will be analyzed by real-time PCR (RT-PCR), to determine the steady state level of the reporter gene mRNA present in the cell for each construct. This will teach us about the correlation between uORF length and NMD.

Risk-Taking Behavior of the Balochistan Gerbil (*Gerbillus nanus*) in Correlation to Testosterone Levels

Jacob Rosenberg
Advised under Dr. Lee Koren and graduate student Chen Naor

Risk-taking is a natural behavior of all animals. Certain individuals, however, take bigger risks. A risk is an activity that has the potential to either be beneficial or detrimental depending on an uncontrollable force. Risks can present themselves in many different facets of life, including reproduction, parenting, and foraging. Previous research shows the management of risky foraging by Allenby's gerbils (*Gerbillus andersoni*). It was observed that the gerbils experienced higher giving-up densities (GUD's) during the larger phases of the moon when the night is brightest and the risk of predation high (Kotler et al., 2010). There are a few ways the gerbils manage the risk of predation when foraging: time allocation, location, and vigilance.

In the present study, trays with food were placed in pairs by specific locations, one in an open area (risky) and one in a bushy area (less risky). Video cameras were placed to capture the gerbils' activity throughout the nights of the full and new moons. Data from the footage was analyzed to determine how much time each gerbil spent looking for predators, foraging, and generally exploring the tray. The longer a gerbil spent alert looking for predators, the less risk it was taking, and the longer it spent foraging without keeping an eye out for predators, the more risk it was taking. GUD was also analyzed to determine at what point the volume of seed in the tray was no longer worth the risk. Data will continue to be gathered and analyzed for an additional year. Hair samples from the gerbils will be processed to quantify testosterone levels in each individual. This allows the comparison of the gerbil's behavior to the influence of testosterone on it. The research is critical in better understanding the coupling of risk-taking behaviors and testosterone.

Kotler Burt P., Brown Joel, Mukherjee Shomen, Berger-Tal Oded, & Bouskila Amos. (2010). Moonlight avoidance in gerbils reveals a sophisticated interplay among time allocation, vigilance and state-dependent foraging. *Proceedings of the Royal Society B: Biological Sciences*, *277*(1687), 1469–1474. https://doi.org/10.1098/rspb.2009.2036

Mov10 in SG and P Bodies

Mordechai Lis
Advised under Prof. Yaron Shav-Tal and Master's Student Gabe Faber

Processing bodies (P-bodies) are distinct cytosolic centers of RNA and protein aggregation within somatic cells that specifically contain many enzymes involved and implicated in processes of mRNA turnover. In a healthy cell, there exists a certain number of P-bodies, but under certain stress inducing environments, such as under amino acid

starvation or serum starvation, cell P-body production rockets upward. The purpose behind this remains to be discovered, but perhaps they act to preserve and guard necessary proteins and RNA transcripts until the stress conditions pass. Stress granules are a related but distinct aggregation that appear under separates stressful conditions from P-bodies, such as an environment containing tubercidin or arsenite, both compounds that are highly toxic to living cells. Stress granule and P-bodies differ not only in what induces their aggregation, but also in their contents and shape and size, with stress granules being much larger and less evenly shaped. Despite their differences, the two structures still have many proteins in common and it is possible they have certain roles in common in times of stress.

One such protein they both share is the Moloney Leukemia Virus 10 protein (Mov10). The full range of Mov10's function and interactions are as of yet uncertain, but it has been implicated as being involved in UPF1 Nonsense Mediated Decay (NMD), a surveillance pathway that functions primarily to reduce error in protein synthesis by eliminating mRNA transcripts that contain premature termination codons (PTCs). One of the projects within my lab is to determine the movement of Mov10 between P-bodies and stress granules and thereby gain a better understanding of their function and of the accumulation of proteins by these structures.

We were able to show that when exposed to P-body inducing environments and then induced to stress granule inducing environments, or vice versa, the Mov10 will move out of the original structure and form new ones. We were also able to capture live movies of this phenomenon as well as perform kinetic analysis using fluorescence recovery after photobleaching (FRAP). Future goals include the production of plasmids that produce PTC RNA transcripts to see if those transcripts colocalize with P-bodies and stress granules with the goal of discovering whether these structures are involved in NMD and resource conservation.

The Role of SIRT6 in Regulation of Exercise Metabolism and Aging Process

Alexandra Tolmasov and Rachel Mauda
Advised under Professor Haim Cohen and M.Sc. student Almog Katz

In the 21st century life expectancy has significantly increased. However, with longevity, many health concerns such as obesity and diabetes arise posing a threat on both life span and health span. The protein SIRT6 may be the solution to avoiding natural consequences of aging. In Prof. Haim Cohen’s lab, we examined the role of SIRT6 under forced and voluntary exercise and the effects of SIRT6 on physical exercise performance.

SIRT6 is located in the nucleus and plays a major role in genomic stability, gene expression, glucose and fat metabolism, stress response, lifespan, circadian rhythm and cardiac hypertrophy. Therefore, SIRT6 protein may be the solution to a healthier longer life. SIRT6 protein is a NAD+ dependent deacetylase, deacylase and a mono (ADP)-ribosylase. In addition to SIRT6 role in whole body homeostasis, Adenosine Mono Phosphate Protein Kinase (AMPK) signaling plays a vital role in metabolic hemostasis and

regulation of healthy life span. SIRT6 was shown to regulate the activity of AMPK.

Male mice overexpressing exogenous SIRT6 (MOSES) had a significant increase in lifespan compared to the wild-type. Insulin-like growth factor (IGF) signaling plays a major role in the regulation of lifespan. MOSES mice showed to have higher levels of IGF-binding protein 1 and altered phosphorylation levels of major components of IGF-1 signaling. Knockout mice, mice that were genetically modified to not express SIRT6, died after a month and suffered from many metabolic disorders. Moreover, they had reduced AMPK activity in muscle.

Physical exercise is defined as planned and structured activity that results from skeletal muscle activation and leads to movement and an increase in energy expenditure. Physical exercise encompasses whole body homeostasis and activates many tissues, organs and physiological systems. Exercise is known to benefit body health; however, more research is needed to elucidate its effect on the aging process mainly on the brain and skeletal muscle. In the project we worked on, we focused on the hippocampus, as it is a source of neurogenesis and memory which are damaged with age and thus connected to longevity. In addition, the hypothalamus was also assessed for comparison as it is a hormonal regulator.

In our experiment, the protein levels in the hippocampus' of three groups of mice were assessed, a negative control group of mice that did not exercise, mice that voluntarily exercised on a running wheel and mice that involuntarily exercised on a treadmill. The physiological changes in these groups were measured using Western Blots in addition to further analyses that were done in order to quantify the blots.

The Western Blots show 293T cells which overexpress more SIRT6 compared to the control (Figure 1).

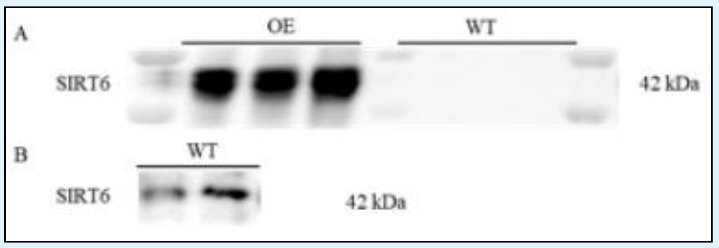

Figure 1: SIRT6 levels in 293T cells, SIRT6 overexpression vs. wild type.
A. SIRT6 overexpression in 293T cells. Due to short exposure time and significant OE, WT SIRT6 was not visible.
B. SIRT6 expression in 293T wild type cells seen after exposing only the WT bands.

In addition, the group of mice that was forced to exercise on a treadmill had no change in SIRT6 levels compared to the control in the liver (Figure 2).

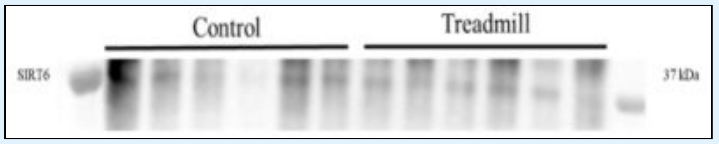

Figure 2: Hepatic SIRT6 levels on control vs. treadmill in WT male mice (age 3 months).

When applying Western Blots on proteins extracted from the brain tissues, it was found that different parts of the brain are affected differently by exercise. The hippocampus of the mice that exercised showed an increase in SIRT6 expression and no change in SIRT1 expression (Figure 3), while the expression of both SIRT6 and SIRT1 was not affected in the hypothalamus (Figures 4A and 4B). There was no significant change in SIRT1, SIRT6 and AMPK between the running wheel and treadmill groups. However, in the running wheel group pAMPK levels stayed the same while an increase in the

TM group was noted compared to the control (Figures 4A and 4B).

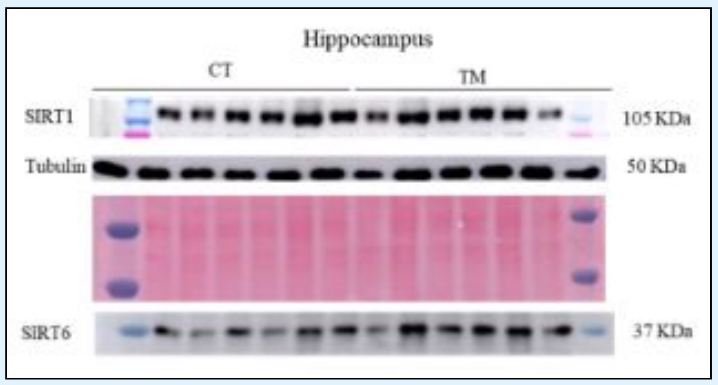

Figure 3: Hippocampal SIRT6 protein expression levels in control vs. treadmill of WT male mice (age 3 months). The ponceau is used as the control.

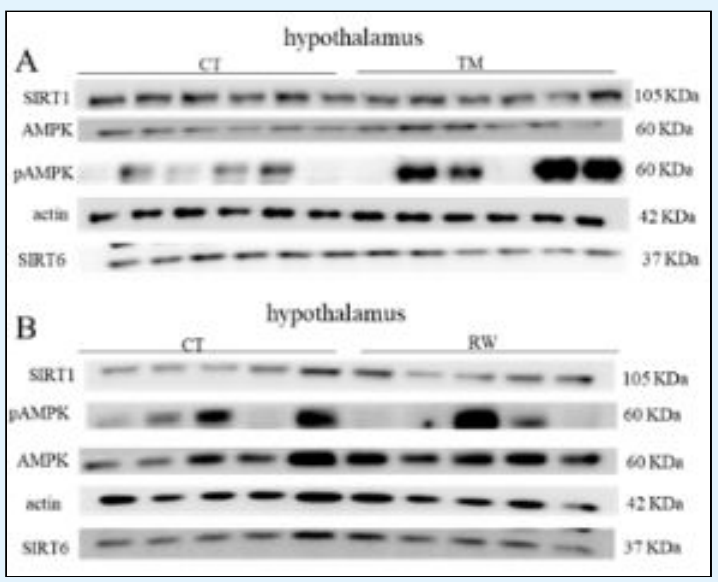

Figure 4: Hypothalamic SIRT6 protein expression levels in WT male mice (age 3 months).
A. SIRT 6 expression levels in control vs. TM group.
B. SIRT 6 expression levels in control vs. RW group.

The Cellular and Developmental Roles of the Essential Protein Codanin-1

Raquel Klinger
Advised under Dr. Benny Motro

Congenital Dyserythropoietic Anemia I (CDA I) is a rare autosomal recessive disorder associated with macrocytic anemia and bone abnormalities. The disorder is caused by a mutation in the *CDANI* gene which encodes for Codanin-1 protein. Our research focuses on the study of the function of Codanin-1 protein. Not much is known about the cellular role of this vital protein. Predictions of Codanin-1's function are further limited by the fact that there are no proteins with a similar genomic sequence to Codanin-1. However, the 3D structure of any protein, as determined by polypeptide folding, hydrophilic and hydrophobic regions, plays a significant role in its function. The predicted 3D structure of Codanin-1 was found to be very similar to the 3D structure of CNOT-1 protein. CNOT-1 has a key role in mRNA stability, translational repression, and transcriptional regulation. Therefore study of the similarities between Codanin-1 and CNOT-1 may allow prediction of cellular function. Furthermore use of CdanR1054W mice, containing the most common human CDA 1 mutation, as an experimental model will allow for the elucidation of Codanin-1's possible involvement in the cell cycle.

Mutated mice were established by using embryonic cells. Embryonic cells grow well in culture and can be experimentally modified. The *CDANI* gene was deleted from the embryonic cells using a process called Cre-Lox recombination; this process is a site-specific recombinase technology, used to carry out deletions, insertions, translocations and inversions in the DNA of cells. Cre-recombinase has the ability to cut out a floxed gene surrounded by two lox P sites. In our research the floxed gene is *CDANI*. Embryos containing an activated Cre protein and floxed Codanin in their genome died within several days of embryogenesis because mice homozygous for the null *Cdan* allele die at an early stage of embryonic development. This leads to the conclusion that Codanin-1 protein is necessary for normal embryonic development. Embryonic

mouse fibroblasts, cells involved in animal connective tissue, with floxed *CDAN1* and inducible Cre were grown in cell culture. Under Cre induction, they were analyzed microscopically and it was determined that they were arrested during cell division. A lower percentage of dividing cells were noted with more heterogeneity in nuclear size and a much higher percentage of bi-nucleated cells. This leads us to assume that Codanin-1 is involved in cellular division. Furthermore the presence of chromatin bridges between the two nuclei indicates that *CDAN1* deletion results in cytokinesis failure.

CNOT1 is a scaffolding protein, which is involved in RNA-related processes including mRNA deadenylation, translational repression and transcriptional control.The significant similar 3D structure of Codanin-1 and CNOT1 suggests similar scaffolding functions for Codanin-1, and possible involvement in similar processes. The major similar structural domains were studied, and identification of interacting proteins bound to these fragments was performed. There are two major approaches utilized to identify these interacting proteins. First, antibodies against Codanin-1 were used for co-immunoprecipitation from HeLa cells, the precipitated proteins were identified by mass-spectrophotometry in the Smoler Proteomics Center, Technion, Haifa, Israel. Protein identification was also accomplished via Tandem affinity purification (TAP). TAP is a form of immunoprecipitation, with the special feature of extracting the protein of interest by tagging it with two high affinity purification tags. In immunoprecipitation only the proteins attached to our protein will precipitate. It is essential to study which proteins bind to determine the similarity between Codanin-1 to CNOT1 and to give us a clue as to what the overall function of Codanin-1 is. C15orf41 is one of two proteins known to be bound to Codanin-1 and for several reasons seems to be very promising in helping to determine the role of Codanin-1. Interestingly, it has been found that a mutation in C15orf41 explains 20% of the cases of CDA1 anemia - the same anemia caused by Codanin-1 mutation.

My area of research focused on further study of C15orf41. Based on C15orf41's sequence it was predicted with high certainty that it is a nuclease, an enzymatic protein that cuts nucleic acids. However, this could allow for many different roles, depending on what type of nucleic acid it cuts. Therefore we decided to produce high quantities of functional C15orf41 protein and incubate it with different types of nucleic acids to see where it would cut. In order to do this we are in the process of producing this protein in a bacterial system that will give a high yield of functional clean protein. In addition, my research involved determining which proteins bind to Codanin-1 on a fragment adjacent to fragment 6, the C-terminal part of Codanin-1, known to bind C15orf41. It is vital to identify and study the proteins that bind to specific areas on Codanin-1, because these proteins may lead to a better understanding of the function of Codanine-1.

Mathematics

(L-R) Front: Jacob Stern, Benjamin Goykadosh, Ezra Splaver
Back: Chemda Wiener, Annette Stawsky

Commutative Subgroups of Braid Group B_3

Annette Stawsky
Advised under Dr. Mina Teicher and Jacob Stern

Braid groups are non-abelian, infinite structures that lend themselves to computationally difficult problems which can be applied to cryptographic schemes. One such problem is the generalized conjugate search problem: given a pair $(x,y) \in B_n \; x\, B_n$ where $y = axa^{-1}$ and $a \in B_m$ for $m < n$, find a.

The generalized conjugate search problem was implemented as a key exchange protocol by Ko, S J Lee, Cheon, Han, Kang, and Park in 2000.

Their scheme relies on two commutative subgroups namely LB_l which consists of all braids generated by the left l strands, and RB_r which consists of all the braids generated by the right r strands.

In a similar vein, our goal was to characterize all commutative pairs of subgroups of a braid group. We approached this problem in B_3 and B_4, the braid groups composed of equivalence classes of braids with 3 and 4 strands respectively. B_3 is structurally very simple because only one of the two properties of braid groups apply, namely that $\sigma_i\sigma_j\sigma_i = \sigma_j\sigma_i\sigma_j$ when i and j are consecutive.

We took two approaches towards characterizing commutative pairs of subgroups, the first involves the intersection of the centralizers of two

elements and the second involves the centralizers of infinitely generated subgroups. We worked first in B_3 with subgroups K and L defined as follows: given two elements a and b in B_3, let $K = Z(a) \cap Z(b)$ and $L = < a, b >$. $Z(a)$ is the centralizer of $a \in B_3$ which means that it contains every element that commutes with a. L is the group generated by any power of any combination of a and b, and their inverses. K and L are commutative since any element of L is composed of a and b which commute, by definition, with any element of K.

Each braid group has a fundamental braid defined as $\Delta_r \equiv (a_1 \dots a_r)(a_1 \dots a_{r-1})(a_1 a_2)a_1$. Artin proved in his original presentation of braid groups that $\Delta_r{}^2$ commutes with every element of B_r. It follows that when K is equal to the fundamental braid squared, $K = \Delta^{2k}$, K and L make a trivial example of a pair of commutative subgroups. The next phase in our research was to characterize all elements a and b for which $K = \Delta^{2k}$.

We successfully simplified this subproblem to determine whether there is a power of b that commutes with a. We prove that $K = \Delta^{2k}$ when $\exists\, m : b^m \in Z(a)$ as follows: B_3 can be represented as $B_3 = \{x, y \mid x^2 = y^3\}$ since one can generate every element of B_3 by allowing $x = \sigma_1\sigma_2\sigma_1$, $y = \sigma_1\sigma_2$. Observe that $x^2 = y^3 = \Delta^2$. It follows that every element of B_3 can be expressed as an even power of the fundamental braid followed by an alternating series of some power of x's and y's. Therefore if we take B_3 modulus Δ^2, we have an isomorphism to the free product between free groups Z_2 and Z_3, $B_3/\Delta^2 \simeq Z_2 * Z_3$. By definition of a free group, the centralizer of any element must consist solely of powers of that element. We showed from there that if s and t are two commutative elements of B_3, then $t = \Delta^{2k} s^n$.

Any finitely generated, commutative subgroups will intuitively be contained in the approach described above and we proved this using induction. Therefore in our search to characterize all commutative subgroups, we were left to explore the remaining possibility of having two commutative, infinitely generated subgroups. Eventually we showed, and found that it had already been shown, that it is impossible to have two commutative, infinitely generated subgroups of B_3. However in the process, we proved a fact that is not immediately relevant to our research: If a group generated by free elements a and b is isomorphic to the free group F_2, then the intersection of their centralizers is a power of the fundamental braid squared.

GRIMM: GRaph IMputation and Matching for HLA genotypes

Ezra Splaver
Advised under Professor Yoram Louzoun

In bone marrow transplants, finding a proper donor-patient match is crucial; an incorrect matching can result in GVHD (graft versus host disease), where the white blood cells from the donor recognize the patient as foreign, and then attack the patient's cells. A large factor in donor-patient compatibility is HLA (human leukocyte antigen) matching within their genomes. Therefore, being able to determine whether any two individuals have the same HLA allele would be of

paramount importance to the care and treatment of those suffering maladies that require bone marrow transplants, such as leukemia.

In my lab, code was written to compute matching between donors and patients. There are two main stages in the code: the imputation stage and the matching stage. The imputation stage tries to predict haplotype pairs from HLA samples that are unphased (the haplotype pair is unclear) and ambiguous (there are multiple possibilities for a single allele). The matching stage then uses the predicted haplotype pairs to determine if there are any matches between patients and donors. As the size of patients and donors increase in the registry, the performance of the computations increases in time. Although code written in the lab runs in sublinear time, which is an improvement over prior code that ran in quadratic time, there is still an issue of calculating results in a reasonable period of time. My job was therefore to further optimize the code's performance.

I looked into a few ways to optimize the imputation stage of HLA matching. Initially, I read up on Numba, which has capabilities to Jit-compile as well as multi-thread parallel processes written in Python, on the CPU and GPU. Unfortunately, I found out that Numba currently has limited support for strings and dictionaries, two data-types that are crucial for the computations. Afterwards, I made several modifications on the code (such as changing data types used, and removing extraneous computations), which helped the code run approximately 40% more efficiently.

Analysis of the structure of Massey Four Products via The Restriction to the Kernel of a Factor

Jacob Stern
Advised under Dr. Eliyahu Matzri

My work this summer revolved around the study of Massey products, which are defined over the Cohomologies of the Absolute Galois Group of a field. Let us take a field F and its algebraic closure F'. Take the Galois group of F' over F and let $\Gamma = Gal(F'/F)$. Let us consider the Homological structures of Γ, assuming the actions of Γ are trivial. $H^1 = Hom(\Gamma \to \mathbb{Z}/p\mathbb{Z})$ and $H^2 \simeq Br(F)$ because of the triviality of the group action. The cup product is a map from $\smile : H^1 \times H^1 \to H^2$. Because of the triviality of Γ, we can assume $x \smile y = x(g)y(f)$. Massey products are an extension of the cup product to three, four or even n inputs.

The definition of the three Massey products on a, b, c all in H^1 is defined as follows. Take two elements $\varphi_{ab}, \varphi_{bc} \in H^1$ such that $\partial\varphi_{ab} = a \smile b, \partial\varphi_{bc} = b \smile c$. (Note: that because of the assumption of the triviality of the group action, $x \smile y = xy$).

Now take $a\varphi_{bc} + \varphi_{ab}c$ now do the same for all of $\varphi_{ab}, \varphi_{bc}\ in\ H^1$. The resulting set is the triple Massey product of a, b, c. Dr. Eliyahu Matzri proved that the Triple Massey product vanishes, that is that the triple Massey product of any three functions in H^1 will always contain 0. The question remains for higher dimension Massey product. My work this summer focused on the Four Massey product.

The Four Massey Product on a, b, c, d is defined similarly to the three Massey product. Find functions, $\varphi_{ab}, \varphi_{bc}, \psi_{cd} \in H^1$ such that $\varphi_{ab}, \varphi_{bc}, \psi_{cd}$

$\partial\varphi_{ab} = a\smile b, \partial\varphi_{bc} = b\smile c, \partial\psi_{cd} = c\smile d$ and they have to follow the following congruences.

$a\varphi_{bc} + \varphi_{ab}c \equiv 0$,

$b\psi_{cd} + \varphi_{bc}d \equiv 0.$

We take those functions and elements and plug them into some function which produces some output, the details of which are not relevant. The Massey four product is the set all the outputs of the above for all $\varphi_{ab}, \varphi_{bc}, \psi_{cd}$ given a, b, c, d.

The study of the Massey products revolves mostly around the indeterminacy (ind) of each product. The indeterminacy is defined as the set of all differences of elements in the Massey product. So on the Massey four product $Ind\,(< a, b, c, d >) = aH^1 + H^1 d + \varphi_{ab}\psi_{cd} - \varphi'_{ab}\psi'_{cd}$.

The first half of the above is quite simple to understand, it is merely two cosets in H^2, it is the second term gives people trouble. This equation is why the actual product is not relevant.

So once the dust settles the real question here is the structure of $\varphi_{ab}\psi_{cd} - \varphi'_{ab}\psi'_{cd} = J$.

My approach this summer was to study this structure by subdividing Γ into cases where $g \in \Gamma\ g \in Ker(x)$, x being one or more of the factors of the product.

If we restrict g to the Kernel of a then $a\varphi_{bc} + \varphi_{ab}c \equiv 0 \Rightarrow \varphi_{ab}c \equiv 0$ and $\partial\varphi_{ab} = a\smile b = 0$ are the only conditions on φ_{ab}. This means that all possible φ_{ab} will form a subgroup call it Φ. Now we can rewrite $\varphi_{ab}\psi_{cd} - \varphi'_{ab}\psi'_{cd}$ as $\varphi_{ab}\psi_{cd} - (\varphi_{ab} + f)\psi'_{cd}$ $f \in \Phi$ and because $\partial\varphi_{ab} = 0$ all elements of Φ can be interpreted as Homomorphisms on $Ker(a)$. So we may further restrict ourselves to the Kernel of φ_{ab} and f then $\varphi_{ab}\psi_{cd} - (\varphi_{ab} + f)\psi'_{cd} = 0$. So now we have (strong) conditions for triviality of J.

This condition, when interpreted as cyclic field extensions of F *or* F_a we get the following tree:

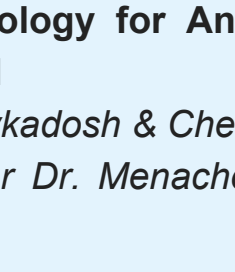

With each of the extensions being trivial cyclic over the previous one. Let G be the Galois closure of F_φ *and* F_a The above tree would clearly imply $Gal(G/F_a) = Gal(F_\varphi/F_a) \times Gal(F_f/F_a) \simeq \mathbb{Z}/p\mathbb{Z} \times \mathbb{Z}/p\mathbb{Z}$.

This means that $J = H^2(Gal(G/F_a) \to \mathbb{Z}/p\mathbb{Z}) = Inf(Gal(G/F_a) \to \mathbb{Z}/p\mathbb{Z}) \simeq \mathbb{Z}/p\mathbb{Z} \times \mathbb{Z}/p\mathbb{Z}$ as long as g is restricted to the Kernel of a. This allows us to say that the indeterminacy of the four Massey product while restricted to the Kernel of a is bounded by some structure, namely $Res_a(Ind\,(< a, b, c, d >)) \subseteq aH^1 + H^1 d + Inf(Gal(G/F_a) \to \mathbb{Z}/p\mathbb{Z})$. Further study is required to see if this result can be lifted to all of Γ.

Voronoi Topology for Analysis of the Vicsek Model

Benjamin Goykadosh & Chemda Wiener
Advised under Dr. Menachem Lazar and Dr. Gil Ariel

In 1995, Tamas Vicsek studied the behavior of bacteria systems and self-propelled particles under specific conditions. The two conditions Vicsek tested were the density of the system and the amount of random movement each

particle in the system underwent (noise). In his experiment, Vicsek showed that under a low density and a high noise, the bacteria system behaves very erratically, with all the particles traveling in random directions. However, at high density and low noise, the particles will align, cluster and move uniformly. These experiments later became known as the Vicsek model (Figure 1). This mathematical model is used to describe active matter and other systems that are able to move on their own. This summer we further investigated the Vicsek model by utilizing a new method of analysis: Voronoi topology.

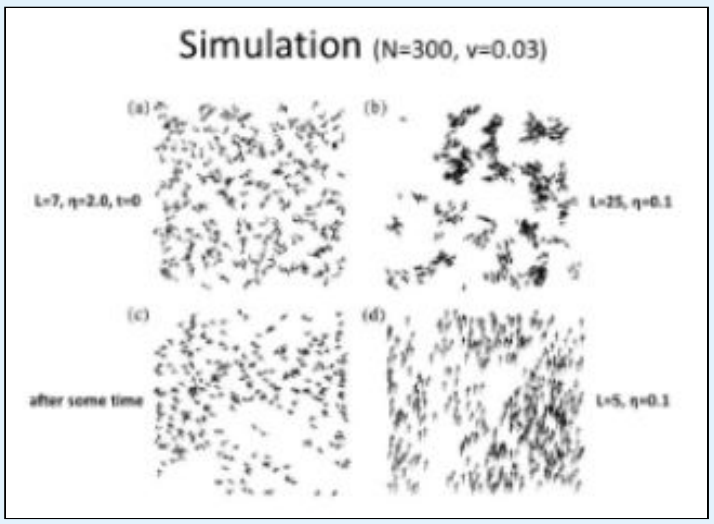

Figure 1: Vicsek's Experiments

Voronoi topology is a type of mathematical graphing that examines the physical arrangement of particles in space. Each particle in the system is bounded by a Voronoi cell, which indicates the region that the particle occupies. These regions are divided by line segments that divide the area based on the distance of one particle to another. For example, the public school system uses Voronoi topology to divide students into the various public schools based on where they live. In this example, the schools represent the particles in the system. Each school receives the students that are closest to their school, with the students on the border becoming the line segment and shared area of the two schools as shown in the image provided (Figure 2).

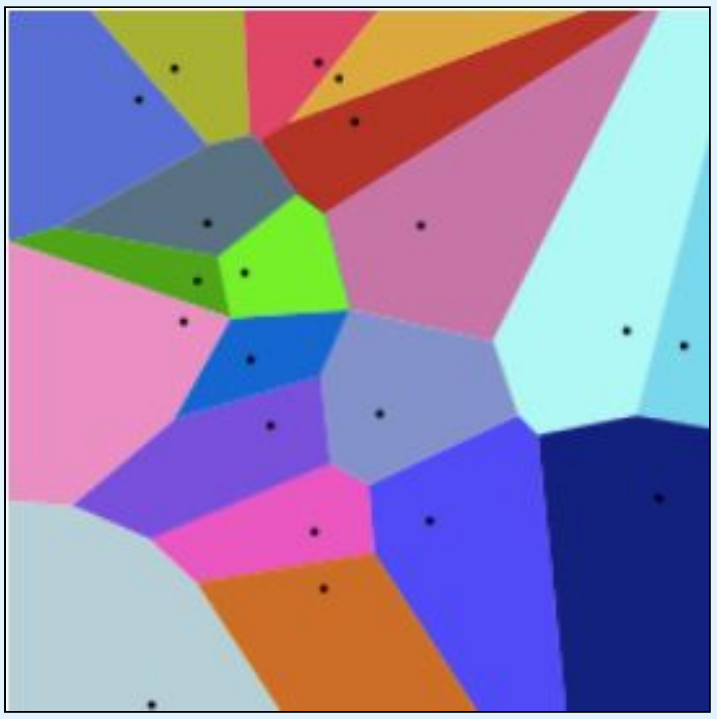

Figure 2: Example of Voronoi topology.

We used Voronoi topology to analyze the Vicsek model to see how the various particles in the system interacted with one another. If all of the particles clustered, as in the case of high density and low noise, we would see that every particle would have a small Voronoi cell area and there would only be a few sides per Voronoi cell. This is expected because like in any circle, the smaller the radius the smaller the circumference: when the particles become so clustered, there are fewer particles physically able to surround a center particle, therefore, there will be fewer sides to the Voronoi cell surrounding the particle. However, if the particles are travelling at random, the Voronoi cell would have many sides because the particles would be further away, thus allowing for more particles to affect it and consequently, more sides to the voronoi cell.

Using the data collected from the simulations of the Vicsek model with Voronoi topology applied, we attempted to compute a graph of the Voronoi shape of each particle and the changes it underwent (Figure 3). We are hoping to find some pattern in the Vicsek model by examining the transitions each particle undergoes and the number of times the Voronoi cell appears in the graph.

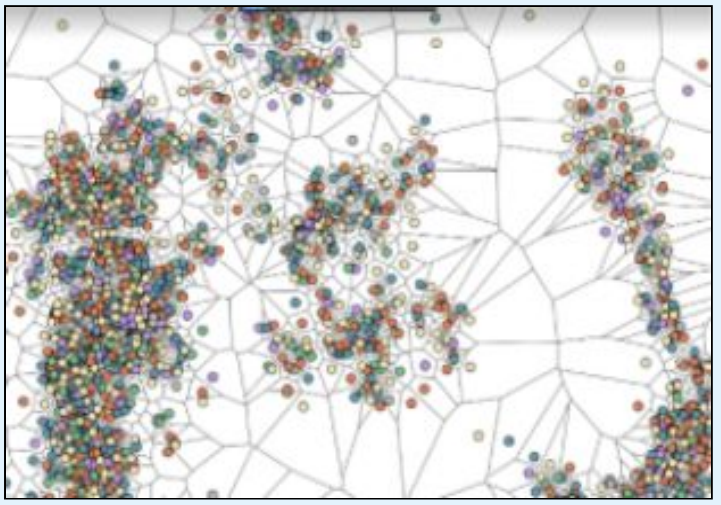

Figure 3: Our simulation incorporating Voronoi topology. This one is under L=25 Noise=2.00

Engineering

(L-R) Hanoch Goldfarb, Zachary Friedman, Max Muss, Jechiel van Dijk, Daniel Ginsburg

Reflectance Thin Film Vanadium Dioxide

Jechiel van Dijk
Advised under Dr. Tomer Lewi

In the phase transition material vanadium dioxide (VO_2), properties such as reflectance and transmission of light can vary drastically with temperature. VO_2 exists in a metallic state and in an insulating state, depending on its temperature. When the temperature of VO_2 is raised above a critical temperature of 67 ^oC, it undergoes a phase transition from an insulating to metallic phase, giving rise to a very large change in its optical constants. When VO_2 is in its metallic state, it is predominantly reflecting light, while the absorption and transmission are rather low (similar to the properties of most metals). In the insulating state, the behavior of the material is like a dielectric, where in general both reflection and transmission are dominant while the absorption is usually very low.

In the experiment light waves were launched at normal incident, towards a 3 layer structure consisting of layers of germanium, VO_2 and sapphire. The germanium was one micron thick, the layer of VO_2 had a thickness of 100 nanometers, and the layer of sapphire was assumed to have infinite thickness compared to the other layers. In the

experiment the reflectance for different normally incident wavelengths was measured, which we can then compare to theoretical results I obtained using Mathematica. By using the transfer matrices method for the 3 layered structure, my results closely agreed with the experimental results.

VO_2 can be used as an active infrared optical component. This will be helpful for designing tunable and reconfigurable flat optical elements. The phase transition property form the metallic to the insulating states of VO_2 can happen as fast as 100 femtoseconds (10^{-15}), which can be used to make ultrafast reconfigurable and reversible optical components.

Graphical Interface for Manipulation of GC-eDRAM Testing Apparatus

Zachary Friedman
Advised under Dr. Adam Teman

Fundamental to the inner workings of modern computers is random access memory (RAM), which is a form of computer storage used to store the machine code intrinsic to executing computer programs. RAM takes a number of forms, which vary primarily in the method by which individual bits, the smallest units of information within a computer system, are stored. Amongst the most popular variants of RAM are SRAM, which relies almost exclusively on transistors to store each bit, and DRAM, which relies on a combination of transistors and capacitors.

The primary drawback of the latter design is the voltage leakage inherent to capacitors, which results in DRAM requiring regular refreshing operations to accurately maintain its values; this leads to a general lack of power efficiency on the part of such memory systems. Bar-Ilan's EnICS lab, however, is developing a novel form of DRAM memory that, while still subject to this flaw, has the capacity to achieve greater efficiency and overall performance than its SRAM counterparts due to its smaller size and reduced bitcell leakage current.

This modified DRAM component, referred to as GC-eDRAM, also has several other advantages, such as not losing its content upon being read, a drawback in traditional DRAM systems. Additionally, its ability to be manufactured in a traditional MOSFET process allows it to be placed on the same die as the processor, allowing for more compact devices that can operate at higher speeds. In addition to this unique form of DRAM, EnICS has developed BEER, a chip to evaluate this new form of computer memory relative to extant variants. This chip is fed instructions by a field-programmable gate array (FPGA), which is in turn manipulated via a complex network of perl scripts.

My role was the creation of a graphical user interface (GUI), as shown in Figure 1, that allows a user to control the FPGA through a display, rather than by running code directly and reading results from command line output. This allows for greater ease of use on the programmer's end, as well as functioning as a demonstrative aid. Additionally, I began the replacement of components of this perl script network with simpler and better-documented python scripts. Creation of the GUI was accomplished via Kivy, a python module that aids in the creation of graphical elements, as well as

a number of python libraries that allowed for the control of perl and BASH scripts. The python scripts used to supplant aspects of the perl script network often functioned in ways fundamentally distinct from the original, but accomplished the same tasks by means of convenient python modules, such as pySerial, which was used to control serial interfaces in setting the voltage supplies that power BEER to desired values.

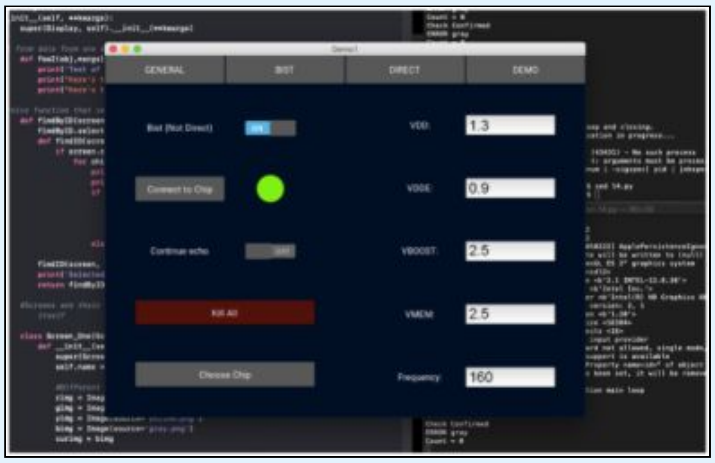

Figure 1: GUI example.

Additionally, a lot of today's components have very regular structures, with plenty of room for optimization in the design process.

To aid in solving these problems, the Emerging Nano-scaled Integrated Circuits and Systems (ENICS) laboratory developed a python library, codenamed "Salamandra", which allows for the creation and easy manipulation of netlists, and can export them into various different formats. My work with Salamandra involved writing functions to query the netlist, such as developing a function to recursively trace the path of a given net to find all of its driving pins. I also did some preliminary research to see if any techniques could be implemented from a somewhat similar project developed by Oklahoma State University called OpenRAM, which designs SRAM netlists in python.

Project Salamandra: A Netlister for Optimized Physical Implementation

Hanoch Goldfarb
Advised under Dr. Adam Teman, Tzachi Noy, and Hanan Marinberg

When designing a computer chip, one of the difficulties that engineers face is organizing the components. To aid in this, there are hardware description languages which formalize the structure and behaviour of the chip as well as its netlist, the list of the chip's physical components and how they are connected together. However, while rigorous, these languages are often cryptic and hard to design in, especially given the size and complexity of many of today's Very Large Scale Integration (VLSI) chips, which often employ millions or billions of transistors.

Searching for Gene Interaction Motifs in Gene Regulatory Networks Through the Use of Model Verification

Daniel Ginsburg and Maxwell Muss
Advised under Dr. Hillel Kugler

As we enter the Information Age, we enter a time when our most valuable commodity is knowledge. So when it comes to genetics, a field that is a foundation for understanding living systems, it is astounding how much we can learn and analyze, especially with the help of computer technology.

Formal Verification is a growing field that has seen major successes in the verification of critical software and hardware systems. It is commonly used in diverse areas such as nuclear power plant safety, airplane engine control, and

hardware chip design. Modern techniques can analyze massive state-spaces while avoiding exponential state explosion by using a symbolic representation of the system.

Accordingly, verification tools are promising as a means to analyze complex biological systems which also suffer from the same state explosion problem. One problem of interest is the analysis of gene interaction within cells. While experimental data can provide the state of various genes at different time points, the actual interactions that lead from one state to the other remains a mystery.

Verification can help solve this mystery. The Reasoning Engine for Interaction Networks (RE:IN) has been developed for this purpose[1]. It reads in an encoding of the biological system as an Abstract Boolean Network (ABN), where critical components (genes) as well as interactions, both known to exist and merely possible, can be specified. Each component can have a list of possible activation functions. The experimental data, consisting of known states of the system at various time points, is read in as well. It then uses the Z3 SMT solver to identify which concrete networks are consistent with the data and if any interactions or activation functions are required or disallowed.

The Backend Reasoning Engine for Interaction Networks (BRE:IN) is an ongoing project intended as a backend to RE:IN. It reads the same model and observation files, but instead performs verification by creating a model in NuSMV, a symbolic model verification language. The experimental data is expressed using temporal logic. The project's long-term goals are to support a wider feature set than RE:IN based on the greater expressiveness of NuSMV, as well as to try to find optimizations to allow the analysis of larger networks[2].

What we have been working on specifically is an additional function for BRE:IN that allows researchers to search the gene interaction model for specific motifs. A motif is a set pattern of interactions between any set of genes. We're hoping that this project can help improve the human understanding of gene interaction on a whole with potential applications in gene therapy, cancer research, antibiotics, pathology, and embryology.

---

[1] Boyan Yordanov, Sara-Jane Dunn, Hillel Kugler, Austin Smith, Graziano Martello, Stephen Emmott. A method to identify and analyze biological programs through automated reasoning, npj Systems Biology and Applications, 2016, Volume 2

[2] Yehuda Goldfeder, Application of Model Verification and Synthesis to Biology, 2018

Physics

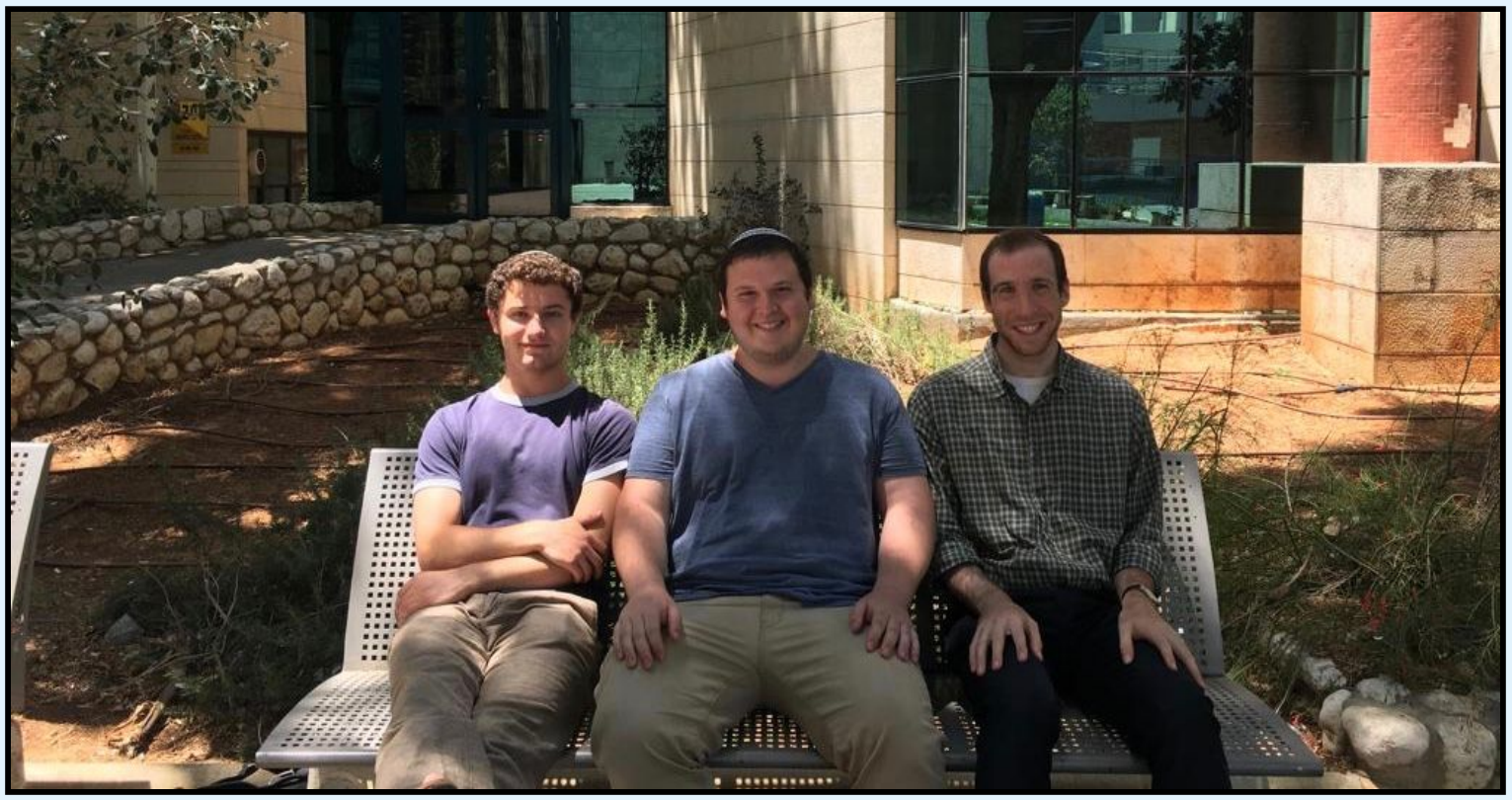

(L-R) Joshua Zak, Jonathan Mamet, Jonathan Tager

Wave Propagation through Disordered Media

Jonathan Mamet
Advised under Prof. Patrick Sebbah and PhD students Bhupesh Khumar, Eli Ashoush, and Master's student Ran Homri

The scattering of waves through disordered media is a paradigmatic phenomenon that has captured the interest of various communities for quite some time now. Among the many important physical aspects of wave propagation that have been studied the phenomenon of Anderson localisation has received particular attention. While much work has been invested into understanding the 'statistical' properties of the corresponding wave phenomena there has recently been a surge of interest in controlling the scattering of waves through 'individual' systems for specific purposes such as detection, imaging, and efficient transmission across disordered materials. Remarkable progress in these endeavors has recently been made in the optical domain, largely due to the availability of spatial light modulators and new concepts for how to apply them on turbid media.

It was recently realized that materials and devices can get entirely new functionalities when adding to them a suitably arranged combination of gain and loss. In particular, structures with a so-called parity time (PT) symmetry were recently introduced theoretically and experimentally in the context of paraxial waveguide optics. On the basis of a delicate balance between gain and loss, these synthetic structures exhibit rich and unconventional behavior, holding promise for numerous applications in nano photonics and lasers.

Here we worked to prove a theory built on the advances that were made in both of the above research fields by combining them in a novel and potentially very useful way. The theory began with three components for a general disordered medium, given by a distribution of the real part of the refractive index nR(x), a corresponding distribution of its imaginary part nI(x) can be found, such that a wave propagating through this medium will feature a constant intensity throughout the entire non-uniform scattering landscape. In other words, the theory proposed that by adding a judiciously chosen distribution of gain and loss to a disordered medium it will make waves lose all of their internal intensity variations such that they propagated through the disorder without any back-reflection. We sought to prove this theory by both physically completing the experiment with the laser being reflected through an actual disordered medium and through the use of simulations through Matlab.

Transport Measurements of 2-D Oxygen-Depleted Regions in $SrTiO_3$

Joshua Zak
Advised by Professor Amos Sharoni, and graduate students Naor Vardi and Ilan Baiman

Strontium titanate (STO) is a band gap insulator and thus a poor conductor in its natural state. When a region of STO is exposed to a sufficiently strong electric field, oxygen vacancies develop, essentially rendering the region metallic and allowing electrical conduction. We sought to characterize how this oxygen-depleted region carries current, specifically whether there are non-uniformities that would not be found in a regular metal, and whether the conductivity is confined to a 2-dimensional layer at the interface. Using a field-effect transistor built onto a substrate of STO, an oxygen-depleted sheet was created by applying a voltage to the gate electrode. A voltage difference was induced between the source and drain electrodes, causing a current to flow through the oxygen-depleted sheet. This setup was subjected to a battery of tests – resistance vs. temperature, hall effect, and magnetoresistance – to ensure that the conducting channel was metallic in nature. The whole apparatus was then cooled to around 2 K to reduce phonon scattering and help in characterizing the intrinsic and quantum properties of the device. The carrier density and transport properties of the STO channel as a function of gating protocol and temperature are being characterized. Further investigation can now be performed with a scanning superconducting-quantum-interference-devices (SQUID) to produce a map of current flow in the oxygen-depleted region.

Low Power Accelerator Particle Detector Concept

Jonathan Tager
Advised under Dr. Yoni Toker

In molecular fragmentation experiments molecules are accelerated to high kinetic energy, then irradiated by a laser, causing them to break up, and the fragments thus produced are counted by a particle detector. By determining the position and time of arrival of the fragments one can determine their original velocity which

allows us to determine the original wave function of the molecule.

The present research focuses on building a sensor that can deduce the velocities of the particle fragments and allow for this calculation to be made. There are two main hurdles that must be overcome. One is that the particles are so small that there must be something that can magnify their impact in order for a sensor to sense them. The other is that the sensor must detect this impact in real time, on the nanosecond timescale.

The solution to the first problem is to use a micro-channel plate detector (MCP). This is a small plate laced with micron sized holes on which a high voltage (typically 2 kiloVolts) is applied. When a particle impacts the MCP, it knocks some electrons loose, and they are accelerated through the tube, banging into the opposite wall and knocking even more electrons loose. At the end of the tube the signal has been amplified several orders of magnitude. By positioning a phosphor screen at the back of the MCP, the electrons exiting the tube create a spot of light as they hit the screen. Thus for every particle hitting the MCP an electronic signal is produced which can be used to time the event, and a spot of light is created which can be used to determine the position of the hit.

The present research is focused on finding a new solution to the second problem. A simple camera cannot operate at a high enough frequency to see where individual particles hit the MCP. It would just see the entire screen lit up by thousands of particles hitting it within one millisecond. The proposed solution is to use a series of avalanche photodiodes, which basically function as one-pixel cameras, but have the required gigahertz refresh rate. Each one will output a single value for the intensity of the light that reaches it at any given time.

There are two possibilities that are being investigated. One is to put a few photodiodes around the MCP and use them to triangulate the location of the signal. Since the intensity of the light is dependent on the distance from the source, the intensity that each of the photodiodes detects can be used to determine where the source is. This concept is similar to the way GPS works today, in that by measuring the distance from several satellites one can calculate the position (Figure 1).

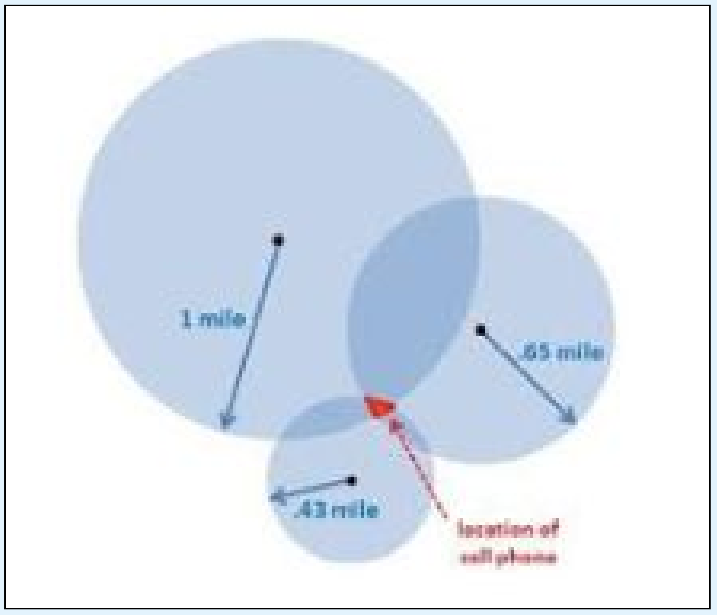

Figure 1: Triangulation is a method of determining position by measuring the distance from three or more distinct points.

The second possibility is to use three photodiodes, each with a different gradient filter in front of it. One will have a gradient filter that cancels any position related differentiation in intensity so that it can be used as a control to see how bright the signal was. This is necessary because the MCP produces signals with random

intensity. The second photodiode has a filter that becomes increasingly dark moving from right to left, showing where on that axis the signal came from. The third photodiode has a filter that darkens from top to bottom, showing where the signal came from on that axis (Figure 2).

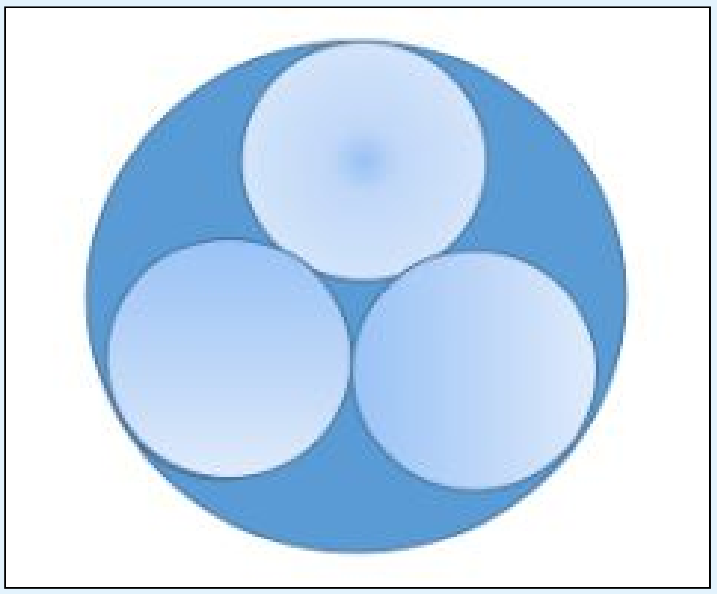

Figure 2: A set of three filters can determine the position. The top one measures signal intensity, the left measures y position, and the right measures x position.

Theoretically, either one of those solutions should work independently. However, both need to be optimized before they can actually be useful in an experiment. There is also a possibility to use both ideas together. If the approximate position can be determined by triangulation, then additional photodiodes placed behind a filter can increase accuracy. If the filters would have several stripes of gradient (Figure 3), then the photodiode would not be able to tell which section of the screen the light is coming from, as each section would have the full range of transparencies, but it would be able to tell where within a section the light landed. If the section was already calculated by triangulation, then this could greatly increase accuracy.

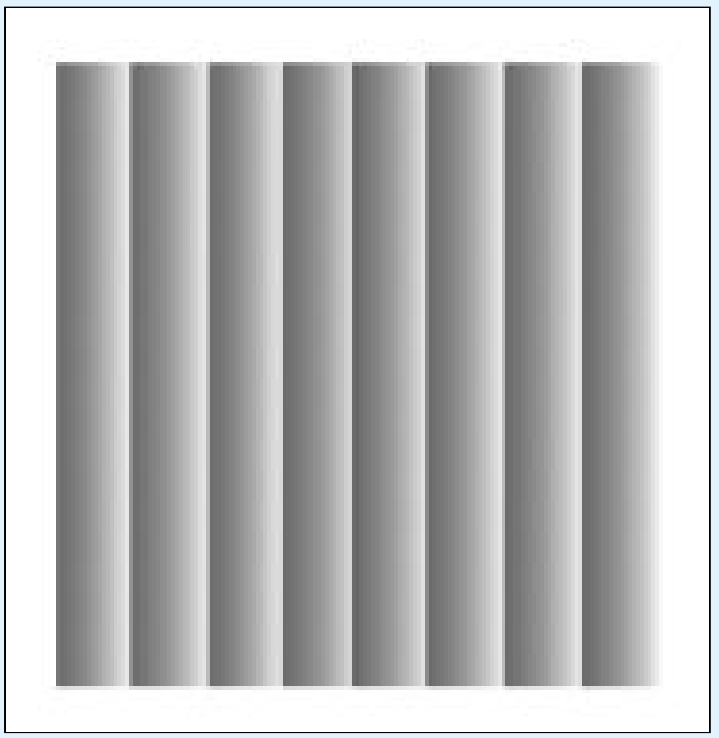

Figure 3: A set of juxtaposed narrow filters can take a fine measurement of position, assuming a coarse measurement is taken by another sensor.

Chemistry

(L-R) Asher Dworkin, Aviva Landau, Michal Mizrahi, Esther Solooki

Electrochemistry: Hydrogen Fuel Cells

Michal Mizrahi
Advised under Professor Lior Elbaz and Dr. Naomi Levy

The conservation of energy is one of the most prevalent issues in the 21st century. Nowadays, most of our energy is obtained from the combustion of fossil fuels. While the combustion process produces energy, it releases many toxins into the atmosphere, which are detrimental to our environment, its climate and our health. With increasing industrialization, elevated pollution levels, and peak global warming rates, it is imperative to develop alternative, cleaner technologies for energy production.

In the search for alternative energy conversion technologies, the objective is to find a technology that is cost-efficient, clean, and reliant on abundant materials. One of the most efficient and clean technologies today is the fuel cell technology. It runs on oxygen and hydrogen and produces only water.

Figure 1 presents a schematic design of a polymer electrolyte membrane fuel cell (PEMFC). By definition, PEMFCs converts the chemical energy stored in the hydrogen molecule into electrical energy. Fuel cells require the use of catalysts in order to carry out the hydrogen oxidation reaction (HOR) and the oxygen reduction (ORR) on the anode and the cathode, respectively, by using a catalyst to increase the ORR kinetics, the overall

power output rises. The most common catalyst used for ORR today is Platinum, homogeneously dispersed on a carbon surface.

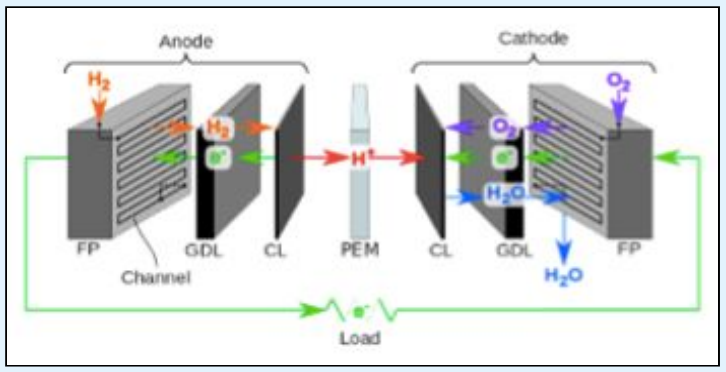

Anode reaction: $H_2 \rightarrow 2H^+ + 2e^-$

Cathode reaction: $O_2 + 4e^- + 4H^+ \rightarrow H_2O$

Overall reaction: $2H_2 + O_2 \rightarrow H_2$

Figure 1: Fuel cell diagram and the reactions that occur. Showing the many layers which each have specific properties vital for fuel cell efficiency.

ORR is considered the bottleneck of PEMFC technology, due to its relatively sluggish kinetics. The focus of this work was to synthesize platinum nanoparticles on carbon support and study their physical and electrochemical properties. The mechanism of ORR catalysis by platinum works by the bonding of the di-oxygen molecule to it and slightly breaking its double bond. The hydrogen protons and electrons are then able to break the rest of the bonds at a much lower activation energy, causing the reaction to happen more efficiently. Although platinum-based materials are considered to be the best ORR catalysts, platinum scarcity and its derived price contributes to about 49% of the fuel cell price. One of the main goals in this research is to lower the platinum loading while maintaining its performance by maximizing its active surface area with smaller Pt particles instead of particles clustering.

The catalyst material synthesized in this work is composed of 20%wt platinum and 80%wt carbon. The carbon surface on which the platinum is impregnated into ensures that the Pt does not grow too large. In this work pseudo allotropic Carbon, Vulcan XC-72, was used. The main characteristics of this carbon is that it is highly porous, allowing the use a method called “incipient wetness impregnation’’ to deposit the platinum on the carbon surface. The platinum is introduced onto the carbon as an aqueous salt, hexahydro-chloroplatinic salt, (H_2PtCl_6). Since the carbon’s pores are so small, capillary action allows the dissolved platinum ions to be pulled into the pores. Then the sample is dried in a tube-furnace overnight while hydrogen gas is purged through it. This hydrogen gas reduces the platinum ions in the salt to metal, and it crystalizes. Being that the platinum is embedded into the carbon’s pores, it is not able to crystalize to particles larger than the pore’s size, and therefore it stays small and has maximum catalytically active surface area.

To ensure that the catalyst was properly prepared, several techniques were used to study the product of this synthesis. X-ray diffraction (XRD) was first used to determine platinum's crystalline structure and size. This method is based on the interaction of X-rays with the material’s crystalline structure, which diffracts the rays in an orderly fashion. The structure of a solid depends on the specific elements that form it, which will tend to solidify in a unique way. This dictates the specific diffraction angles obtained from the XRD. By comparing the peaks (Figure 2) to expected literature for platinum and its different plane

orientations, it is evident that the peaks match the values of cubic platinum crystals. This confirms that the platinum in our sample has indeed crystallized into its optimal structure. By applying Bragg's law to compare the wavelengths of the projected X-ray and the diffraction angle, along with the Scherrer equation, the size of the particle was calculated at the peak's full width at half maximum on average to be the microscopic size of 1.64 nm. After calculating that the particles are small, it is still necessary to do further analysis to ensure that the small particles are homogeneously dispersed and did not form larger aggregates. Transmission electron microscope (TEM), that projects a ray of electrons at extremely high voltages, allowing us to have high magnification and resolution of the sample. Carbon and platinum are distinguishable in the image due to the fact that platinum is a heavier element than carbon and not as many electrons can pass through it, causing it to appear darker. Figure 3 indicates that the platinum particles stayed as small, separate units, that are homogeneously dispersed throughout the sample.

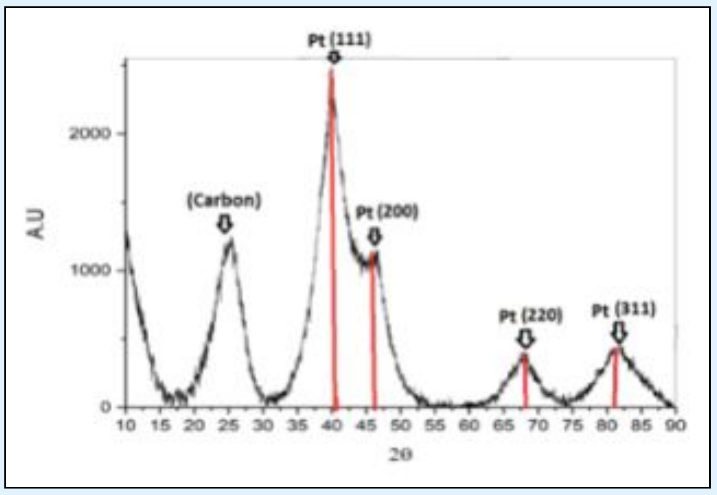

Figure 2: Diffraction peaks obtained from the XRD of Pt-C sample.

Lastly the sample's catalytic activity was studied using a rotating ring disk electrode (RRDE). The electrode was plated with the catalyst sample, then placed in an acidic solution (0.5 M H2SO4) saturated with oxygen, and set to cycle between two potentials. The graph below depicts the ORR with and without Pt present. The results show platinum's significance in the reduction of oxygen. Without the platinum, depicted by the black line, the ORR hardly happens and if it does it is only when reaching a very high potential. When platinum is present however, depicted by the blue line, the reaction occurs at a much lower overpotential, lower activation energy and there is a significantly larger current.

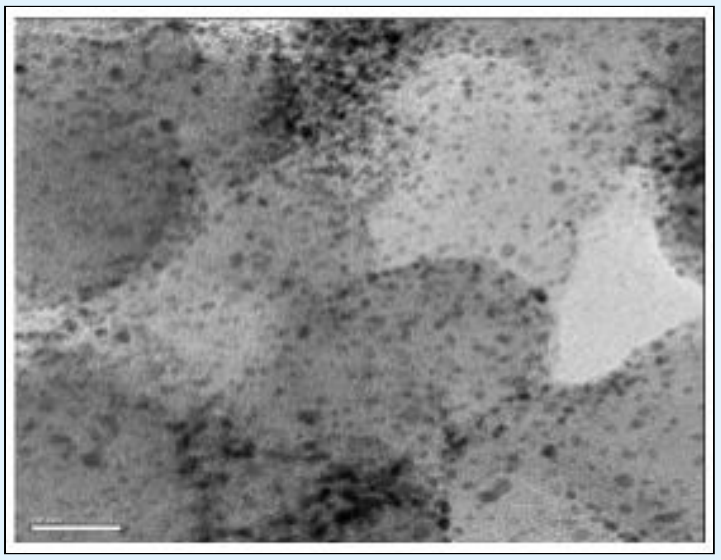

Figure 3: TEM images at 20nm Bar of Pt-C sample.

This research proves the significance of the Pt in the catalyst in fuel cells and shows how the overall amount of Pt can be reduced through maximizing its active surface area while still obtaining the same efficiency.

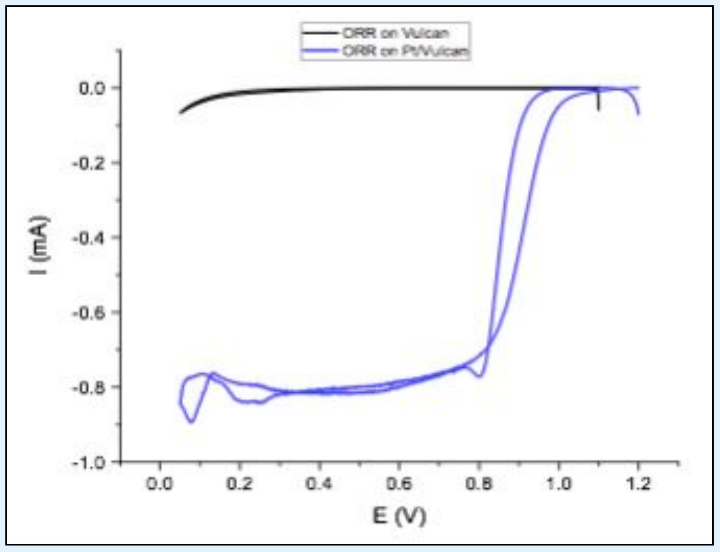

Figure 4: Comparing RRDEs of Vulcan and Platinum with Vulcan in H2SO4 solution.

NMR Investigation on the Impact of WIP upon ubiquitylation of WASP

Aviva Landau
Advised under Professor Jordan Chill and research student Saja Baloum

Wiskott Aldrich Syndrome (WAS), a rare X-linked recessive immunodeficiency disease, is caused by a mutation that affects the production of Wiskott-Aldrich Syndrome Protein (WASP).[1] WASP aids in the regulation of the actin cytoskeleton which is important for many hematopoietic and immune cell functions.[2] Previous studies show that WASP-Interacting Protein (WIP)'s C terminal contains a multi-epitope WASP binding domain, which attaches to the N-terminal EVH1 domain of WASP, thus stabilizing WASP's inactive closed confirmation. Phosphorylation of WIP tyrosine residues Y455, Y468 and Y475 results in partial dissociation of the WIP/WASP complex and activation of WASP. In this state, WASP is also open to ubiquitination-triggered proteasomal degradation.[3,4] It is unclear why WIP's partial release of WASP is responsible for the degradation of WASP as the lysine amino acids that ubiquitin attaches to (K76 and K81) are relatively exposed regardless of WIP's position. This project examines a possible explanation: before ubiquitin covalently tethers to the two lysines, it binds *non-covalently* to a WIP-shielded location as a first step towards tethering.

To conduct this experiment both a wildtype and a triple Y-to-E mutant WIP-WASP complex were expressed and isolated. The mutant complex was created with glutamic acid, an accepted phosphomimicking residue, replacing the three aforementioned tyrosine residues. Additionally, both protein complexes were expressed in growth culture containing the ^{15}N isotope so that they could be analyzed using a Nuclear Magnetic Resonance (NMR) spectrometer. Since amino acids in the protein each contain one ^{1}H-^{15}N pair, they each give rise to a single cross-peak in the ^{1}H-^{15}N two-dimensional NMR spectrum, allowing us to observe changes in the electronic environment which typically result from protein-protein contacts. After running the 2D-NMR spectrum for the two different protein complexes and observing the pattern of cross-peaks, ubiquitin (a 76-residue protein) was added to each of the protein complex solutions and the 2D-NMR experiment was repeated. The results were compared to determine which amino acids (if any) ubiquitin has an effect on when WIP partially releases WASP, and to conclude roughly where (if at all) ubiquitin attaches before tethering.

As expected, the NMR spectrum of the wildtype WIP-WASP complex did not change after the addition of ubiquitin. However, the triple mutant WIP-WASP complex spectrum also did not change after the addition of ubiquitin, thus

indicating that when WIP partially releases WASP, ubiquitin does not non-covalently bind to WASP before tethering. It is still possible that ubiquitin non-covalently binds to WASP, but no change was seen on the spectrum since the complex used in this experiment was phospho-mimicking the wildtype complex. It is also possible that the non-covalent binding is so weak that it does not appear as a change on the spectrum, but this explanation is unlikely. Alternatively, it is possible that the enzyme ligase which is responsible for the binding of ubiquitin to lysine, before performing its function, non-covalently binds to WASP where WIP partially releases WASP. This would explain why no change was seen with the addition of ubiquitin, and why WASP is only open to ubiquitylation-triggered proteasomal degradation when WIP uncovers part of WASP. Future research needs to be done to further investigate the structure of the WIP-WASP complex and how the proteins interact with one another, and perhaps this research will reveal the answer.

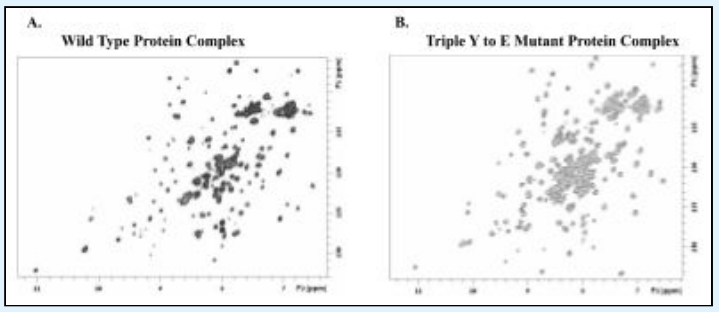

Figure 1: NMR Spectrum
A. NMR spectrum comparing the wild type WASP-WIP protein complex prior and post the addition of ubiquitin. Dark grey represents the complex prior to the addition of ubiquitin and light grey represents the complex after the addition of ubiquitin.
B. NMR spectrum comparing the triple Y to E mutant protein complex prior and post the addition of ubiquitin. Dark grey represents the complex prior to the addition of ubiquitin, and light grey represents the complex after the addition of ubiquitin.

[1] Derry, J. M., J. A. Kerns, U. Francke. 1995. WASP gene mutations in Wiskott- Aldrich syndrome and X-linked thrombocytopenia. Hum. Mol. Genet. 4:1127–1135
[2] Derry, J. M., Ochs, H. D. and Francke, U. 1994. Isolation of a novel gene mutated in Wiskott-Aldrich syndrome. Cell 78:635.
[3] de la Fuente, M. A., Y. Sasahara, N. Ramesh. 2007. WIP is a chaperone for Wiskott-Aldrich syndrome protein (WASP). Proc. Natl. Acad. Sci. USA. 104:926–931.
[4] Fried, S., Reicher, B., Pauker, M. H., Eliyahu, S., Matalon, O., Noy, E., Chill, J. and Barda-Saad, M. 2014. “Triple-Color FRET Analysis Reveals Conformational Changes in the WIP-WASp ActinRegulating Complex.” Science signaling 7(331):ra60.

Studying the Effects of pH on CueR, the Copper Efflux Metalloregulator

Esther Solooki
Advised under Prof. Sharon Ruthstein, and research students Hila Sameach and Renana Kaufman

Maintaining homeostasis is a basic and necessary function for both prokaryotic and eukaryotic organisms. In the proper concentrations, metal ions play an integral role in facilitating essential cellular processes. At the same time, however, their toxicity in high concentrations is lethal to all organisms. In the human body, copper is required for proper neurotransmitter function in the brain, but accumulation of this metal can lead to neurodegenerative diseases. Prokaryotic systems require copper ions as cofactors for enzymes that catalyze oxidation reduction reactions taking place within their cells. As in humans, an improper concentration of copper will lead to the cells’ death. Microorganisms have therefore developed sophisticated systems devoted to regulating the concentration of metal ions in their environments. The Ruthstein lab is studying copper homeostasis mechanisms in both the human body and *E. coli* – which is used as a model because of its

presence in the human system. The lab hopes that a more thorough understanding of these copper regulation cycles will aid in the development of new antibiotics. These drugs will work to kill the bacteria while ensuring the safety of a human host.

The Ruthstein lab is now studying the effects of pH levels on CueR, the copper efflux metalloregulator protein present in *E. coli*. CueR comes from the MerR family of proteins, which is comprised of domains for DNA and metal ion binding. Metalloregulators are cytoplasmic or transmembrane proteins which bind to specific metal ions with high affinity and play a role in regulating the concentration of these metal ions within the cell. CueR, a transcription factor, is able to induce or repress the expression of two specific genes through metal binding. In its repressed form, CueR bends DNA in a way that prevents RNA polymerase from binding to the promoter, thus stunting transcription. When copper ions bind to CueR, however, a conformational change occurs. The protein, now in its active state, allows for RNA polymerase to bind to the promoter region of the DNA strand. Once transcription is initiated, the expression of two genes begins and consequently two proteins are formed. The first is CopA, an ATPase, which pumps Cu^{+} from the cytoplasm to the periplasm. The second is CueO, the copper oxidase, which oxidizes the toxic Cu^{+} to the less toxic Cu^{2+} ion.

We studied the effects of pH on CueR in four states: unbound (apo), bound to copper (holo), bound to DNA (repressor) and bound to copper and DNA (activator). In order to discern structural changes or denaturation of CueR caused by pH, we employed the use of two methods: continuous-wave electron paramagnetic resonance (CW-EPR) and circular dichroism (CD) spectroscopy. In order to obtain a spectrum of CueR through EPR, we spin label the protein with paramagnetic centers. Thus, as the constant magnetic field B_0 excites the unpaired electrons to jump to a higher spin state, the system measures and records electrons' reflection of the power. EPR spectroscopy also allows us to study our protein in solution. We are therefore able to study CueR while it is free to move, as it is able to within the cell. Through this technique, we can record hyperfine interactions – the interactions between unpaired electrons and the nucleus. This helps in determining the polarity of the labeled region of the molecule and how its folding is affected due to changes in pH. Additionally, if exchange interactions between nearby electrons are visible in the spectrum, EPR measurements allow us to discern the formation of aggregates in solution, showing that the protein is unstable in the given environment (Figure 1). CD spectroscopy is a type of light spectroscopy which emits circularly polarized light in 2 directions. It is used to study the structure of asymmetric biological molecules. The peptide bonds between amino acids of the protein absorb the incoming rotating light. The absorbance changes based on the conformation or structure of the protein. We are thus able to detect any changes in the secondary structure of the protein – alpha helix or beta pleated sheets (Figure 2).

These two methods allow us to understand the behavior of a protein in

specific conditions. We can detect protein flexibility and changes in conformation due to the instability of the protein in a given environment. The knowledge of the dynamics of the protein is essential in order to fully comprehend the biological system. Further data, however, must still be collected.

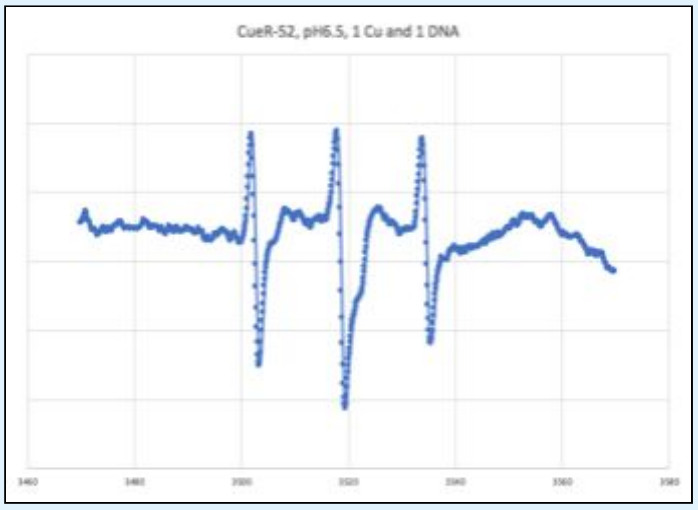

Figure 1: EPR Spectrum for CueR
The smaller peaks found in between the three main peaks may indicate the formation of aggregates in solution.

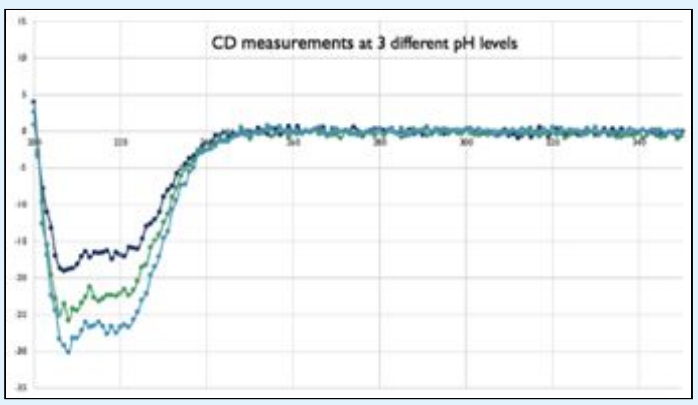

Figure 2: CD Spectrum of CueR at pH 9.5 (dark blue), 8.5 (green), 7.5 (light blue).
The spectrum shows no changes in the secondary structure of the protein, which is primarily made of alpha helices.

Changela, A., Chen, K., Holschen, J., Outten, C.E., O'Halloran, T.V., and Mondragon, A. (2003). Molecular basis of metal-ion selectivity and zeptomolar sensitivity by CueR. Science *301*, 1383–1387.

Wladron, K.J., Rutherford, J.C., Ford, D., and Robinson, N.J. (2009). Metalloproteins and metal sensing. Nature *460*, 823–830.

Raman Spectroscopy and Atomic Force Microscopy of Nanoparticle Monolayers

Asher Dworkin
Advised under Dr. Yaakov Tischler

The field of nano-photonics describes the study of light matter interactions at nanoscale. Dr Tischler's lab is currently working on a variety of goals mainly focusing on nanophotonics and spectroscopy. Particular areas of interest include using spectroscopy techniques to analyse lasing, characterize monolayers and obtain Raman spectra of different materials.

A crucial element of the lab is the ability to prepare samples with layers of nanoparticles of different materials with thickness of a few nanometers on a variety of substrates from silica glass and silicon to materials with functional coatings. Various functional nanoparticles are used in sample preparation. Needless to say, there are multiple methods of preparation. Four primary methods of preparation used in the lab include: Physical Vapour Deposition, Dip Coating, Spin Coating and Langmuir-Blodgett deposition.

At Tischler's lab monolayer and multilayer deposition in liquid phase are carried out using the Langmuir-Blodgett deposition technique. Monolayers are of primary interest as they allow laser probing of in-plane and out-of-plane functional group in organic molecules. This gives a better understanding of the fundamental vibrational modes and their characteristics when extended with Raman Spectral analysis in-situ. The principle of the Langmuir-Blodgett technique is to deposit amphipathic

molecules (containing hydrophilic and hydrophobic heads and tails), to form a nanoparticle layer onto a surface of a sub-phase (water). The nanoparticles arrange themselves with hydrophobic tails held above the water and the hydrophilic head immersed in water. The Langmuir Blodgett trough barriers subsequently compress the layer on the water until the nanoparticles are condensed down. This must be done at a slow rate in order to assure maximum conformity of the nanoparticles. The substrate used for this project has generally been silicon or glass, pre-treated in differing ways depending on sample requirement. The substrate is dipped into the sample once compression is complete and is coated with a layer of nanoparticles.

Following preparation of the samples, the samples were characterised. The two key techniques employed in characterising the sample are Raman spectroscopy and Atomic force microscopy (AFM).

Atomic force microscopy is a standard technique used for analyses of topography of nanoscale samples. It operates using an oscillating tip at a resonant frequency and monitoring the damping effect of the combination of forces from the material as the sample draws near the surface. This gives an image of the topography of a small section of the sample at a resolution of the order of fractions of nanometres, typically that of the diameter of the tip.

Additionally, Raman spectroscopy uses monochromatic laser excitation to obtain scattered photons. Upon filtering the Rayleigh scattered photons, i.e. the photons scattered at the same frequency/ wavelength as that of the excitation laser, the Raman scattering effect is observed through a spectrograph. The observations on the spectrum infer the chemical make-up of the surfaces. In this process the energy of the incident coherent photon is used to excite the material to a higher virtual energy state, as a result of excitation, relaxation emits photons primarily of the same wavelength as the input, and also with a shifted wavelength. Such an emission has an infinitesimally small probability, which is of the order of 0.0001%, which is fairly detectable and highly relevant. The spectrum of the wavelength emitted from the excited analyte gives a unique spectrum, which serves as a signature or fingerprint of the material make-up.

Having analysed the sample with Raman and AFM an accurate picture can be constructed of the sample topography and nanomaterial composition can be confirmed. Understanding substrate analyte interactions is very crucial in drawing a baseline for all the analysis, may it be of academic or industrial interest. These material specific monolayer fabrication and general characterisation techniques employed at Tischler’s group throw flood lights on this less researched domain of greater impact.